2017-01-01

Electronic Structures of Magnetic Endohedral Fullerene And Application of Self Interaction Correction to Atoms

Kamal Nyaupane
University of Texas at El Paso, kkamal.nyaupane@gmail.com

ELECTRONIC STRUCTURE OF MAGNETIC ENDOHEDRAL FULLERENES AND APPLICATION OF SELF-INTERACTION CORRECTION TO ATOMS

KAMAL NYAUPANE

Master's Program in Computational Science

APPROVED:

Tunna Baruah, Ph.D., Chair

Rajendra Zope, Ph.D.

Ming-Ying Leung, Ph.D.

Charles H. Ambler, Ph.D.
Dean of the Graduate School

Dedication

To my parents

Deu Narayan Nyaupane and Late Durga Devi Nyaupane

ELECTRONIC STRUCTURE OF MAGNETIC ENDOHEDRAL FULLERENES AND APPLICATION OF SELF-INTERACTION CORRECTION TO ATOMS

by

KAMAL NYAUPANE

THESIS

Presented to the Faculty of the Graduate School of

The University of Texas at El Paso

in Partial Fulfillment

of the Requirements

for the Degree of

MASTER OF SCIENCE

Computational Science Program

THE UNIVERSITY OF TEXAS AT EL PASO

December 2017

ACKNOWLEDGEMENTS

Any intellectual work is never a result of an individual effort. Mine is not an exception to this. In the process of finalizing my work I would like to thank all those people who gave me the scholarly guidance and emotional support during my work and even outside of the work.

First of all, I would like to express my deepest gratitude to my advisor/supervisor Prof. Dr. Tunna Baruah, Department of Physics, University of Texas at El Paso. It is an great experience for me to work under her supervision in this lab. Her constant guidance, important suggestions and encouragement is the influential force behind the success of this work.

I would also like to express my deepest gratitude to my Co-Supervisor Prof. Dr. Rajendra Zope, Department of Physics, University of Texas at El Paso, for his continuous guidance and for continuous thoughtful suggestions.

Special thanks to Dr. Luis Basurto, Dr. Yoh Yamamoto and Mr. Sushil Bhusal for their utmost help, encouragement, valuable comments during the work. I am really thankful to my friends Mahesh Koirala, Pawan Koirala, and brother Sabal Ranabhat for their co-operation throughout the work.

No words are satisfactory to express my gratitude to my father Deu Narayan Nyaupane, my sister Dhan Kumari Nyaupane, my brother Prakash Nyaupane and my Spouse Neelam for their unconditional love and support all the time.

ABSTRACT

Endohedral fullerenes, which represent a novel family of carbon nanostructures, are fullerene cages with atoms, ions or clusters trapped in their cavities. The encapsulated molecule or cluster can determine the properties of the fullerenes as charge transfer often occurs from endohedral unit to the outer cage leading to high stability. Endohedral fullerenes hold a lot of fascinating properties with potential applications in biomedicine, molecular electronics and photonics etc. In this work, novel endohedral fullerenes containing transition metal oxide cubane cluster are studied for possible magnetic properties. The motivation is to examine whether the encapsulation can lead to stabilized transition metal clusters with high magnetic anisotropy energy. The electronic and magnetic properties of $Co_4O_4@C_{70}$, $Co_4O_4@C76$, $Co4O4@C_{78}$, $Co_4O_4@C_{80}$, $Mn_4O_4@C_{70}$, $Mn_4O_4@C_{76}$, $Mn_4O_4@C_{78}$ and $Mn_4O_4@C_{80}$ are calculated using density functional theory. The magnetic anisotropy energy of these endohedral fullerenes is calculated using a perturbative approach for including the spin-orbit interaction.

The density functional theory calculations employ approximations to the exchange-correlation functional, which are not free from self-interaction. The self-interaction leads to delocalized d-orbitals and can lead to incorrect spin states in some systems. We test the recently developed self-interaction correction scheme based on Fermi-Lowdin orbitals. The final motivation is to apply the scheme to transition metal based systems. In this proposal we present the preliminary work done using the Fermi-orbital based scheme to closed-shell atoms. In future, this work will be extended to transition metal oxide clusters.

TABLE OF CONTENTS

CHAPTER 1

INTRODUCTION

Scientific work can be divided into two parts: one is experimental, in which two elements of experiment are equipment and operation and the other is theoretical. Experimental research may consume a lot of monetary resources and the operation demands human beings to face potentially dangerous materials. Also, some hypothesis cannot be directly tested experimentally. So computational method can be the good replacement being safe and inexpensive.

Numerous computational methods were developed along with the development of the modern computers. In computational physics, based on Newtonian mechanics, there is a molecular dynamics method used to study large molecules like proteins. Other methods are constructed on quantum mechanics which are useful to the study of electronic structure and properties of the molecules. Density functional theory (DFT) formalism is our main theme here. If we wish to study the electronic structure and the properties of an interacting system such as electrons in a molecule or solid, we have to consider many electron wave function i.e. $\psi(\overrightarrow{r_1},\overrightarrow{r_2},\dots\dots\overrightarrow{r_N})$, $\vec{r_i}$, which denotes the electrons' co-ordinate and spins [1]. We underline the structure and properties of specific materials rather than universal properties of all, and here, total energy and its component is important. Currently the most popular method is DFT in quantum physics and chemistry, hence we focus on DFT in this thesis.

With the combination of low computational cost and accurate results, DFT is one of the most useful and promising approach in quantum physics to study the large and

complex molecular system. DFT has established itself a leading method to study the magnetic and electronic properties of molecules. It faces some problems in some applications caused by approximate exchange correlation functional and electron self-interaction introduced by approximate density functional [2].

Using the approximate functional in exchange correlation part results self-interaction error (SIE). SIE is the residual interaction of an electron with itself. SIE comes from the self-interaction in the exchange part and the coulomb part cannot cancel each other exactly.

Since this work highly discusses about fullerene, the major composition of this research, it is highly important to go over its introduction.

1.1 Discovery of fullerene

For the first time, Fullerenes were discovered in September 1985 [3]. The number of carbon atoms ranged from 20 to hundreds in fullerene. C_{20} is the smallest fullerene. Fullerenes are hollow closed carbon cages which consist of hexagons and pentagons that has three-fold co-ordination. We need exactly 12 pentagons to make the fullerene closed. Hence, C_{20} is the smallest fullerene cage possible as it is composed of exactly 12 pentagons. To make bigger cages, we can increase the number of carbon atoms with different pentagonal and hexagonal arrangements. The Bucky ball, which has 60 carbon atoms, is the most popular one named after Buckminster Fuller. This fullerene was first observed by the group of scientists, Richard Smalley, Robert Curl and Harry Korto, at Rice University, Houston and they were awarded with Nobel prize in 1996 for their novel discovery. The first fullerene discovered was C_{60}. Total number of isomers of C_{60} is 1812 with different arrangements of pentagons and hexagons, in which one has

icosahedral symmetry. Fullerene is further hybridized into exohedral and endohedral. However, this thesis focuses on the endohedral fullerene.

1.2 Endohedral fullerene

Immediately after the discovery of fullerene in 1985, scientists proposed that fullerene can encapsulate some atoms, molecules, ions or clusters inside it because of its completely closed cage nature.

Endohedral metallo-fullerene are an interesting class of fullerenes because the charge transfer can occur from encaged unit to the carbon cage and this dramatically alters the properties of the fullerenes [4].

The first metallo-fullerene was presented by the joint research group from Sussex University-Rice University in 1985. They concluded that lanthanium atom can be encaged within the fullerene. It was the first discovery of concept of Endohedral metallo-fullerene. They first tried with Fe and failed to encapsulate. The encapsulated unit plays important role for the electronic and magnetic properties of the endohedral fullerene. Depending upon the endohedral unit, endohedral fullerene can be differentiated as non-metal doped fullerene, metallo-fullerene and molecular endo-fullerene. Endohedral fullerene has a wide application as a contrast agent in MRI in biomedicine, magnetic memory in electronics and various other forms in many research fields depending on the unit inside it.

With the presence of metallic species and also the strong interaction of endohedral unit with the fullerene, the electronic properties and the structures differs explicitly with those of fullerene only. Due to this unique chemical properties, research on it has expanded vastly encompassing various fields.

An important feature of endohedral fullerene is the electron transfer from inside clusters to the cage, which produces novel structure, properties and potential use of these hybrid molecules. The number of electron transfer from metal to cage differ depending upon the cluster properties.

1.3 Mechanism of endohedral fullerene

Usually the production mechanism of endohedral fullerene through two methods experimentally, they are

1. Ion bombardment method:

   With this mechanism small atoms or ions such as H^+, He may directly penetrate through pentagonal or hexagonal rings of fullerene and stay inside the fullerene cage to form endohedral structure but for large atoms or ions the five or six membered rings is too small to pass inside.

2. Arc discharge method:

   In this method, the arc is discharge by using vaporizing graphite/metal composite rods in helium atoms. This is a widely used method for the production of metallo-fullerene.

Since the goal of this research is to make magnetic material using metal oxides as an endohedral unit, it is crucial to discuss the idea of magnetism.

1.4 Magnetism

In our daily lives magnetic materials plays an important role. Magnetism was first discovered by ancient Greeks and used by the Chinese to make a “south pointing” compass. Some applications of magnetic materials include frictionless bearings, medical devices, magnetic separators, loudspeakers, microphones, sensors, switches,

storage devices, generators and motors. The widespread commercial possibility of magnetic materials has driven research in this particular area.

Traditional magnetic materials are composed of two or three dimensional arrays of inorganic atoms, transition metals that contains spin magnetic moments. To produce this kind of material we use metallurgical methodologies in very high temperatures.

The transition metals are the elements of periodic table which have a partially occupied d orbital by electrons.

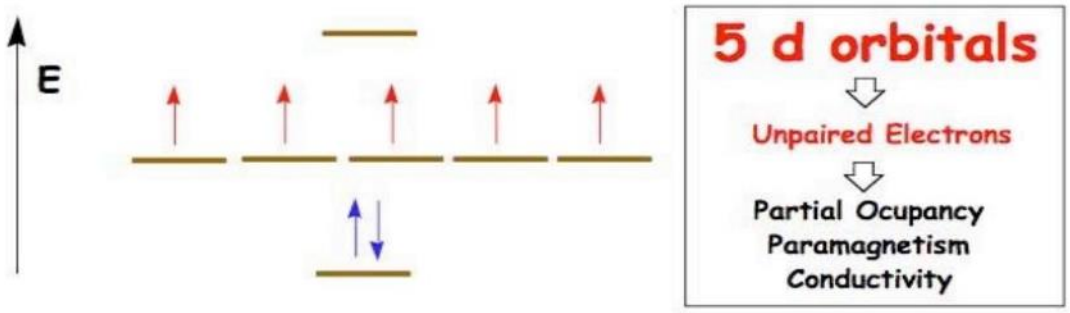

Fig. 1. The d orbitals of transition elements are at the origin of the magnetic, conducting and optical properties of those elements.

1.5 Classes of magnetic materials

The best way to present the different types of magnetism is to define how the materials respond to magnetic fields. All matter is magnetic some are much more magnetic than others.

The magnetic behavior of materials can be classified into the five major groups:

1. Diamagnetism
2. Paramagnetism
3. Ferromagnetism

4. Anti-ferromagnetism
5. Ferrimagnetism

Diamagnetism is based on the interaction in between magnetic fields and the electrons. All materials are diamagnetic because all material contains electrons [5].

Diamagnetic substances are those substances which are feebly repelled by a magnet. Diamagnetic materials create an induced magnetic field in a direction opposite to an externally applied magnetic field and they are repelled. There are no permanent dipoles in diamagnetic materials. Some properties of diamagnetic materials are

- when diamagnetic materials brought near the pole of a strong magnet it experiences a repelling force.
- the magnetic susceptibility χ of these materials is always negative.
- the relative permeability μr is always less than one.
- in the absence of external magnetic field, the net magnetic dipole moment is zero.
- Examples: Bismuth, Copper, Lead, Zinc etc.

Using one of the five major classes of magnetism, we can describe the magnetic behavior of material. These classes are described according to how the adjacent magnetic moments would interact with each other at absolute zero.

Interaction for all four classes are shown below in the figure.

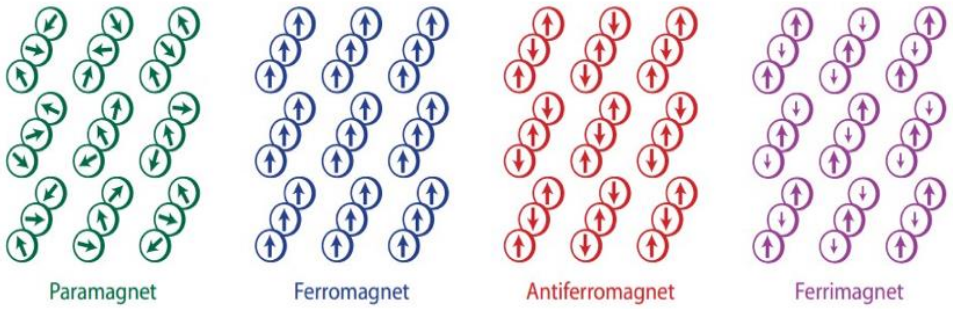

Fig 2. The alignment of magnetic moments for all four classes of magnetism at absolute zero.

For paramagnets, no adjacent alignment is observed. Ferromagnets show parallel alignment of adjacent magnetic moments. Anti-ferromagnets show antiparallel alignment and the Ferrimagnets exhibit antiparallel alignment and are composed of two magnetic spins of different strength.

Paramagnetic substances are those which are feebly attracted by a magnet. It results from the presence of atoms that have permanent magnetic moments. Paramagnetic materials exhibit magnetism when the external magnetic field is applied and tend to line up with the field. The basic need for paramagnetism in solid is some degree of isolation in the individual magnetic dipole moments.

In ferromagnetic material, parallel alignment of adjacent magnetic spins which results in a large net magnetic moment even in the absence of magnetic field. The magnetic moments in these materials exhibit very strong interaction with applied fields.

Two distinct features of ferromagnetic materials are:

- Spontaneous magnetization
- Magnetic ordering temperature i.e. Curie temperature

  Below the curie temperature, the ferromagnet is ordered and above it, disordered.

In antiferromagnetic materials, magnetic spins alignment are anti-parallel that results in a material with no net magnetic moment. Anti-ferromagnetically alignment is analogous to the process of bonding and thus, is favorable. Anti-ferromagnetism is the most commonly found bulk magnetic behavior.

In ferromagnetic materials, the adjacent magnetic spins have an antiparallel alignment with different magnitudes. The resulting material shows net magnetic moment in the absence of an applied magnetic field. Ferrimagnetism is a special case of anti-ferromagnetism since the material consists of an alternating spins of different magnitudes.

So, magnetic material has a memory effect that is very useful for constructing memory devices. Here, we are going to investigate the magnetic material that can be used for magnetic storage devices and has many other applications. The magnetic material discussed above carries an anisotropy energy which is calculated for the potentiality of making storage devices.

1.6 Magnetic anisotropy energy

Magnetic anisotropy energy (MAE) is the energy required to change the magnetic moments from easy to hard direction inside a crystal. Magnetic material takes a stronger field to magnetize in a specific direction compared to other materials. To get a magnetic saturation, depending upon the orientation of the field with respect to the crystal lattice, one would need a different magnetic field strength. This leads to the two types of axis in the crystal, easy axis and the hard axis, due to the interaction of the spin magnetic moment with the crystal lattice [13].

Directionally specific energy is known as the anisotropy energy, hence "directionally dependent". Magneto-crystalline anisotropy is the most common form of anisotropy energy [13,14].

Likewise, directional dependence magnetic anisotropy is the material's magnetic properties [14]. The magnetic moment of magnetically anisotropic materials will tend to align with an "easy axis", which is an energetically favorable direction of Spontaneous magnetization. The two opposite directions along an easy axis are usually equivalent, and the actual direction of magnetization can be along either of them.

To have a hysteresis in ferromagnets, magnetic anisotropy is a pre-requisite, otherwise it is supermagnetic.

The main cause of anisotropy energy is the spin orbit coupling. In quantum mechanics, the spin orbit coupling is an interaction of a particle's spin with its motion.

The electron has orbital angular momentum l and has a spin s. There is a magnetic moment associated with each angular momentum i.e. spin magnetic moment μ_s and orbital magnetic moment μ_l. Interaction between μ_s and μ_l is the spin orbit coupling.

$$\mu_{l=I\times A}$$

Where I is the current and A is the area of orbit.

We know that time period of the orbital motion of electron is,

$$T = \frac{2\pi}{w}$$

Also

$$I = -\frac{e}{T}$$

Substituting T in above equation, we will get

$$\mu_l = -\frac{ew}{2\pi} \square r^2$$

And we know angular momentum is defined as,

$$|l| = \lfloor r \times p|$$

we know, $P = mv$

$$v = wr$$

$$|l| = mwr^2$$

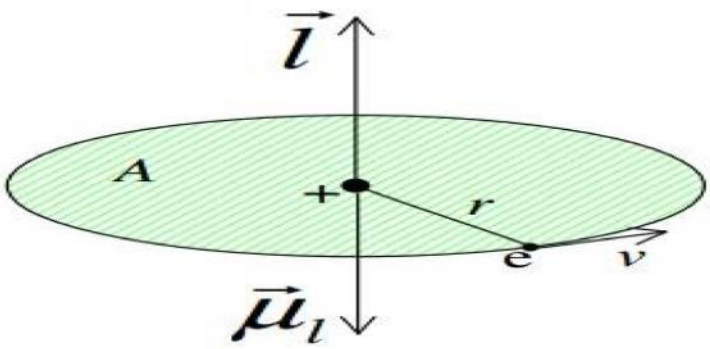

Fig 3. Orbital Motion of electron.

Finally,

$$\mu_l = -\frac{e}{2m}\vec{l}$$

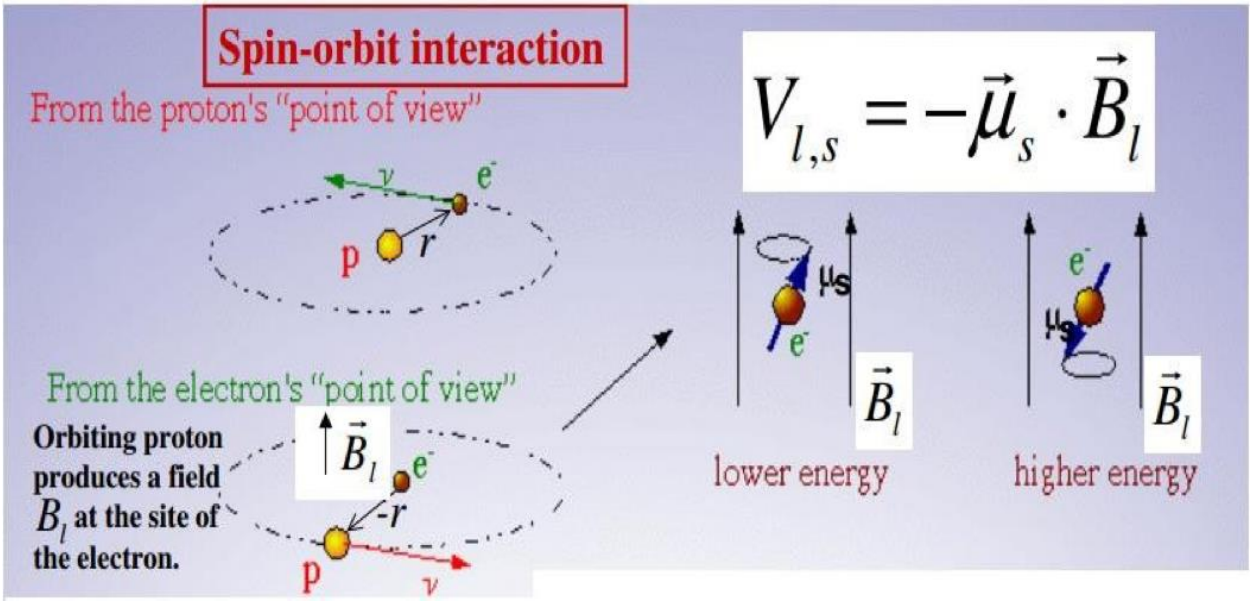

fig 4. spin-orbit interaction

1.5.1 Magnetic moment

In an external magnetic field, magnet will experience the torque. The magnetic moment of a magnet is a quantity that determines the torque. It is considered to be a vector quantity having a magnitude and direction. Most precisely, it is a system's magnetic dipole moment. The mathematical relationship is given by,

$$\tau = \mu \times B$$

Where τ is the torque, μ is the magnetic moment and B is the external magnetic field.

1.5.2 Calculation of magnetic anisotropy energy

I already mentioned that the cause of magnetic anisotropy primarily originates from spin orbit coupling and in the order of micro-hartree. Considering electron is not spinless and moving with velocity v, the interaction is written as,

$$U(r,p,s) = -\frac{1}{2c^2}\, S.P \times \nabla_{\varphi}(r)$$

Where, p is the momentum operator and φ_r is the coulomb potential.

For the numerical solution of Schrödinger equation, we have to determine the spin-orbit coupling matrix element of the form [15].

$$U_{J,\sigma,k,\sigma'} = \langle f_j \chi_\sigma | U(r,p,s) | f_k \chi_{\sigma'} \rangle$$

$$= \sum_x \frac{1}{i} \langle f_j | V_x | f_k \rangle \langle \chi_\sigma | S_x | \chi_{\sigma'} \rangle$$

The calculation of magnetic anisotropy energy was conducted with density functional theory implemented in Naval Research Laboratory Molecular Orbital Library (NRLMOL) code. The density functional theory and methodology for MAE calculation is further discussed in next chapter.

CHAPTER 2

THEORY AND METHODOLOGY

2.1 Density functional theory

Density functional theory is one of the most successful method to investigate the electronic structure and properties of the matter. It is computational quantum method used to examine the electronic structure of atoms, molecules and also complex systems. It has become very useful and popular among the computational field due to its efficiency and considered to be more accurate to predict the electronic structure, potentials, vibrational frequencies, ionization energies, binding energy, band structures of solids, polarizability of dielectric materials, anisotropy energy of magnetic materials, and so on. Hohenberg-Kohn theorem and Kohn sham equations are the main fundamental concept of density functional theory [1,2].

According to quantum mechanics, the primary goal of it is to find the wave function that contains all the information of the system. Once we know the wave function of the system it is easy to study the system's properties. The Schrödinger equation for single electron acted upon an external potential V(r) takes the form,

$$\left[\frac{-\hbar^2}{2m}\nabla^2 + v(\boldsymbol{r})\right]\Psi(\boldsymbol{r}) = E\Psi(\boldsymbol{r})$$

where, the first term is the kinetic energy, second term is the potential energy and E is the energy eigenvalue.

The fundamental aspect of density functional theory is to find the ground state properties of the system by using ground state electron density.

If we know the ground state electron density we can predict all the properties of the system. We can write the electron density as,

$\rho\ (\boldsymbol{r_1}) = \int \psi^*\ (r_1,r_2,.....r_N),\ \psi\ (r_1,r_2,.....r_N) dr_2\ dr_3\ .....dr_N$

In quantum mechanics, system's wave-function contains all the information. With the help of that, we can calculate the expectation values of operator. The binding of electrons appears in atoms, molecules, clusters and so on because of nuclear-electron interaction. The potential energy V(r) acting on the electron is the effect of nucleus or nuclei on the system.

For N electron system, we can write the Schrodinger equation as

$\left[\sum_i^N \left[\frac{-\hbar^2}{2m}\nabla_i^2 + v(r_i)\right] + \sum_{i<j} U(r_i, r_j)\right]\psi(r_1 r_2 \ldots . r_N) = E\psi(r_1 r_2 \ldots \ldots r_N)$

properties of the system including the energy E, can be expressed as functionals of the electron density i. e. they are determined by a knowledge of the density alone.

The exact energy functional for DFT:

$$E^{DFT} = T_s[n] + U_{col}[n] + U_{ext}[n] + E_{xc}[n]$$

To solve the Schrodinger equations for N electron system, there are numerous powerful method like perturbation theory and configuration interaction method, but they are less efficient for large and complex system. Though DFT is less precise, it gives practical alternatives for the case where we need to analyze the properties of a large system. DFT tells us that for all the non-relativistic coulomb systems differ only in their

external potential i.e. v(r) and gives the way how to deal with the operators $\hat{T}$ (kinetic energy operator) and $\hat{U}$ (Potential energy operator).

2.2.1 Some problem in DFT

If we can find the exact exchange-correlation functional, we can say DFT is exact but the exact functional is not available. Due to the approximate functional in DFT, there are some problems.

The orbital energy calculations of DFT are somewhat useless caused by wrong asymptotic behavior of the approximate functional. Orbital energies are not able to reflects real physical quantities such as ionization energy. Due to the interaction of electron with itself, also called self-interaction introduced by functional, DFT produce wrong results when we applied to the open shell systems [2]. There will be more or less self-interaction error in those exchange-correlation functional.

2.2.2 The Hohenberg-Kohn theorems

Basics of density functional theory are the two Hohenberg-Kohn theorems. The first states that "the external potential V_{ext}(r) is a unique functional of ρ(r); since in turn external potential fixes Hamiltonian. We see that the full many particles ground state is a unique functional of ρ(r)". With this theory we can write the ground state electronic energy as [2, 8].

$$E_0[\rho_0] = T[\rho_0] + E_{ee}[\rho_0] + E_{Ne}[\rho_0]$$

In the above expression the first term is kinetic energy, second term is the potential energy due to electron-electron interaction and the last term is the potential energy due to coulomb interaction between electrons and nucleus.

In the second theorem it proves the variational principle held for electronic ground states; “The functional that delivers the ground state energy of the system, delivers the lowest energy if and only if the input density is the ground state density”. With this for an N-electron system,

$$E_0 \leq E[\rho] = T[\rho] + E_{Ne}[\rho] + E_{ee}[\rho]$$

Where, ρ is any trial density. DFT is now also applied to the study of excited state not only the ground state.

2.3 Kohn-Sham equation

Kohn-Sham reformulated the system in such a way that the interacting electrons system is replaced by non-interacting fictitious particle system i.e. each particle experiences an average potential due to all the other electrons. In the exchange correlation functional, all the interaction, like correlation and exchange between the particles, are included. Kinetic energy can be expressed in terms of orbitals. The set of equations leads to the variational process known as Kohn-Sham equations. The ground state charge density for a system of non-interacting particle is,

$$n(r) = 2\sum_i |\psi_i\,(r)|^2$$

Where ψ_i(r) is the kohn-sham orbital, which are the solution of the Schrodinger equations.

$$\frac{-\hbar^2\nabla^2}{2m} + V_{ks}(r) = \in_i \psi_i(r)$$

or we can write

$$\left[\frac{-\hbar^2}{2m}\nabla^2 + v(r) + v_H(r) + v_{XC}(r)\right]\psi_i(r) = \epsilon_i\psi_i(r)$$

The KS orbital must obey certain constraint.

To get the density, KS introduce an orbital like equation,

$$\left[-\frac{\hbar^2}{2m}\nabla^2 - \sum_A Z_A\frac{e^2}{|r-R_A|} + e^2\int\rho(r')\frac{1}{|r-r'|}dr' + U_{xc}(r)\right]\psi_i = \mathcal{E}_i\psi_i$$

The first term of the equation is the kinetic energy, second term is the nucleus electron interaction and the third and fourth term being the coulomb potential and exchange correlation potential respectively. Implementation of Kohn-Sham procedure is to, first, choose a basis functions and write a molecular orbital as a linear combination of the basis functions times the coefficients i.e.,

$$\psi_j = \sum_i C_{ji}\,x_i$$

Where C_{ji} are the coefficients and x_i are the basis functions. To get the electron density we need to sum up all the orbital densities of occupied orbitals.

$$\rho = \sum_{j=occ} n_j\big|\,\psi_i(r)|2$$

we use this density to find the potential. Once we know the effective potential we can solve the KS equations. This process is continuing till the convergence is reached.

We have the KS energy expression,

$$E[\rho] = \sum_{j=occ}\left\langle\varphi_i\middle|-\frac{\hbar^2}{2m}\nabla^2|\varphi_i\right\rangle + \int\rho(r)V(r)d^3r + \frac{e^2}{2}\int\rho(r')\rho(r)\frac{1}{|r-r'|}d^3r'd^3r + E_{xc}[\rho]$$

The exact functional form of exchange correlation energy is not known and hence various approximations to this functional exists.

From the above discussion, we are trapped with the problem of how to define the exchange correlation function. In this DFT calculation, GGA (generalized gradient approximation) is used, which has all the information from both local electron density and local density gradient. There are numerous GGA functions; among all, here we used Perdew-Burke-Ernzerhof (PBE) functional implemented in the parallel NRLMOL code [9].

2.4 Variational principle

In quantum mechanics, variational principle is one of the method for finding approximations to the lowest energy eigenstate or ground state, and also some excited states. This allows the calculation of approximate wave functions such as molecular orbitals. The root for this is the variation theorem [10].

This theorem explains that the expectation value of the energy for any trial wave function is equal to or greater than the ground state energy. This result gives a very powerful means of obtaining an upper bound to the exact ground state energy [5].

A widely useful approximation method is the variational method. This method is the basis of quantum chemistry, Hartree-Fock theory, density functional theory and variational quantum Monte Carlo [11].

The basic idea of this method is to guess a trial wave-function, which consists of some adjustable variational parameters. These parameters are adjusted till the energy of the trial wave-function is decreased. The resulting trial wave-function and its corresponding energy are variational method approximations to the exact wave-function and energy [11,12].

We can prove this easily. Let the trial wave-function be denoted by Φ. We can magnify the trial wave-function as a linear combination of the exact eigen-functions, which is denoted by ψ_i. In practice, we don't know the ψ_i since we're supposing that we're employing the variational method to a problem which we can't solve analytically. The trial wave-function can be written as

$$\Phi = \sum_i c_i \psi_i$$

And the energy analogous with this wave-function is given by

$$E[\Phi] = \frac{\int \Phi^* \hat{H} \Phi}{\int \Phi^* \Phi}$$

In an exact wave-function substitute the expansion we will get,

$$E[\Phi] = \frac{\sum_{ij} {c_i}^* c_j \int {\psi_i}^* \hat{H} \psi_j}{\sum_{ij} {c_i}^* c_j \int {\psi_i}^* \psi_j}$$

we know the Eigen-function of Hermitian operator form an orthonormal set.

5.6 Computational method

All electron theoretical calculations were carried out within the density functional formalism. Our density functional based computations were implemented with the all-electron Gaussian-Orbital based Naval Research Laboratory Molecular Orbital Library (NRLMOL) program using PBE GGA to describe the exchange correlation effects.

CHAPTER 3

SELF-INTERACTION METHODS

3.1 Self-Interaction Correction

In this chapter self-interaction correction for the atomic system will be given. SIE is the one error that come from the construction of most approximate exchange-correlation functional, which comes from the interaction of electron with itself.

Precise knowledge of electronic properties is necessary for the application of microelectronic devices. To calculate these properties density functional theory has been established as an extremely useful method. Although the density functional theory in principle is exact, the exchange-correlation energy is unknown and therefore needs to be approximated. Among all the approximations most are semi-local approximations that assumes that at a given point the exchange-correlation energy only depends on the density and the derivatives of the density. The use of approximate exchange-correlation functional results in self-interaction error (SIE), which arises from the fact that the self-coulomb is not exactly canceled out by the self-exchange term and some residual self-interaction remains [16]. The self-interaction error does not arise in the Hartree-Fock theory where the exchange term is calculated exactly. The presence of SIE results in a number of problems in predicted properties such as band gap, lattice constant, dissociation curve, reaction barriers, fragment charges, charge transfer excited states, Rydberg states, d-state and f-state localization etc. [2,15].

The self-interaction problem in DFT was pointed out by Perdew and Zunger in a seminal paper published in 1981. The self-interaction correction (SIC) suggested by

Perdew and Zunger handled the problem by presenting orbital dependent correction to the XC energy functional as:

$$E_{XC}^{SIC}[n_{\uparrow}, n_{\downarrow}] = E_{XC}[n_{\uparrow}, n_{\downarrow}] - \sum_{\sigma}^{} \sum_{i}^{N_{\sigma}} \{U[n_{i\sigma}] + E_{XC}[n_{i\sigma}, 0]$$

where E_{XC} is the exchange-correlation energy of a system containing n up and n down electrons, U is the coulomb energy, σ is the spin index and N_{σ} is the number of occupied orbitals. The self-interaction corrected total energy of the system is

$$E^{SIC-DFT} = E^{DFT}[\rho_{\uparrow}, \rho_{\downarrow}] - \sum_{i\sigma}^{} \{U[n \sum_{\sigma}^{} \sum_{i}^{N_{\sigma}} \{U[n_{i\sigma}] + E_{XC}[n_{i\sigma}, 0]\} F \quad [\rho_{\sigma}$$

Perdew and Zunger used this approach for calculations on atoms using atomic orbitals. However, any straight-forward similar applications using Kohn-Sham orbitals in larger systems such as molecules, solids, 1-and 2-dimensional periodic systems becomes complicated due to the size consistency problem. In an extended system the Kohn-Sham orbitals becomes more and more extended as the system size increases. Thus, the SIC correction to energy, which will be non-zero in an isolated atom, will become vanishingly small per atom in an extended system. To achieve the size consistency, the correction term is orbital dependent and as a result the total energy is not invariant under unitary transformation within the occupied orbital space. Thus the Kohn-Sham orbitals cannot be used for calculation of SIC in a multi-atom system and localized orbitals need to be used. It was demonstrated by Harrison, Heaton and Lin that wannier functions in solids, which are localized functions constructed from Bloch functions, yield self-interaction corrections of same magnitude as in atoms. Pederson et.

Al. [16] showed that the local orbitals that minimize the self-interaction corrected energy need to satisfy the equation

$$\langle \phi_{i\sigma} | V_{i\sigma}^{SIC} - V_{j\sigma}^{SIC} | \phi_{j\sigma} \rangle = 0$$

also known as localization equation, apart from the eigenvalue equations

$$\{H_{0\sigma} + V_{i\sigma}^{SIC}\} | \phi_{i\sigma} \rangle = \sum_{j} \lambda_{ij}^{\sigma} | \phi_{j\sigma} \rangle$$

Due to the additional pairwise localization equations, the self-interaction correction calculations tend to be slow and therefore are not widely used. The initial applications were on small molecules that showed promising results [17].

The local orbitals can be obtained from a unitary transformations of the occupied orbitals. The localized orbitals should also be the set that minimizes the total energy. The advantage in using fermi orbitals is that they are dependent on a quantity which is unitary invariant – density matrix. A Fermi orbital is just the ratio of one particle spin density matrix to the square root of spin density:

$$F_i(r) = \frac{\rho(a_i, r)}{\sqrt{\rho(a_i)}}$$

$$F_i(r) = \frac{\sum_{\alpha} \psi_{\alpha\sigma}^{*}(a_{i\sigma}) \psi_{\alpha\sigma}(r)}{\sqrt{\{\sum_{\alpha} |\psi_{\alpha\sigma}(a_{i\sigma})|^2\}}} = \sum_{\alpha} F_{i\alpha}^{\sigma} \psi_{\alpha\sigma}(r)$$

Here $a_{i\sigma}$ are called the Fermi orbital descriptors.

The fermi orbitals are normalized, span the same space of the Kohn-Sham wave-functions but they are not orthogonal to each other by construction. In the applications

they are orthogonalized by following the Lowden's orthogonalization scheme. In the applications, the first step to find the descriptor positions which will generate N_σ linearly independent local orbitals. The set of FOs are then Lowden orthogonalized. The third step is to minimize the energy as a function of the FOD is achieved by calculating the "forces" on the FODs from the equations:

$$\frac{dE^{SIC}}{da_m} = \sum_{kl} \lambda_{kl}^{k} \{\left\langle \frac{d\square_k}{da_m} \middle| \phi_1 \right\rangle - \left\langle \frac{d\phi_1}{da_m} \middle| \phi_k \right\rangle\} \equiv \sum_{kl} \lambda_{kl}^{k} \Delta_{lk,m}$$

The FOD positions are updated using a conjugate-gradient scheme till the forces are smaller than a predetermined threshold.

The optimization of FODs is however, a non-trivial task. The initial guess of the FODs need to be made judiciously. To elucidate how the FODs changes depending on the exchange-correlation, we have carried out initial calculations on a few close shell atoms. These results are described in the chapter 4.

$$E_{XC}^{SIC}[n_\uparrow, n_\downarrow] = E_{XC}[n_\uparrow, n_\downarrow] - \sum_{\sigma} \sum_{i}^{N_\sigma} \{U[n_{i\sigma}] + E_{XC}[n_{i\sigma}, 0]$$

Where σ is the spin index and N_σ is the number of occupied orbital.

Perdew and Zunger expression for a spin-polarized system is,

$$E^{SIC-DFT} = F^{approx}[\rho_\uparrow, \rho_\downarrow] - \sum_{i\sigma} F^{approx}[\rho_{i\sigma}, 0]$$

$$\rho_\sigma(r) = \sum_i [\phi_{i\sigma}(r)]^2 = \sum_\alpha [\psi_{\alpha\sigma}(r)]^2$$

Localized orbitals is given by, $\rho_{i\sigma}(r) = [\phi_{i\sigma}(r)]^2$.

Here is the alternative two step procedure for minimization of energy to solve for the localized orbitals must satisfy:

$$\{H_{0\sigma} + V_{i\sigma}^{SIC}\}|\phi_{i\sigma}\rangle = \sum_j \lambda_{ij}^{\sigma} |\phi_{j\sigma}\rangle$$

$$\langle \phi_{i\sigma} | V_{i\sigma}^{SIC} - V_{j\sigma}^{SIC} | \phi_{j\sigma} \rangle = 0$$

To avoid solving the localization equation and rebuild unitary invariance, localized orbitals can be derived from the fermi orbitals which is classically electronic position. However, determined from the density matrix [18].

CHAPTER 4

RESULTS AND DICCUSSION

Carbons form planar graphene sheet in which the orbitals are in sp^2 hybridization forming covalent bonds with three nearest neighbors. The graphene sheet is made up of hexagons. By adding pentagons to the sheet curvature in the sheet can be introduced. To form a closed carbon cage, according to Euler theorem, we need exactly 12 pentagons with hexagonal rings. Fullerenes are carbon cages that are formed by exactly 12 pentagons mixing with different number of hexagons given by the Euler's theorem.

The discovery of C_{60} marked an important step in the advances of nano-materials. Soon after the discovery, it was proposed that C_{60}, which has a diameter of 7.1 A^0, can encapsulate atoms or small molecules. Early experiments identified various atoms entrapped inside the C_{60} under different experimental condition and methods. Later on, a host of endohedral fullerenes of various carbon cage sizes was discovered. The endohedral carbon fullerenes are found to encapsulate various units some of which are not even stable when isolated. For example, the $Sc_3N@C_{80}$ molecule is the third most abundant carbon fullerene but the Sc_3N unit or the C_{80} itself are not stable when isolated. The endohedral fullerenes offer the possibility of developing functional materials for targeted applications through encapsulation.

In this project, we are exploring the possibility of designing magnetic molecules through exploring possibilities for the endohedral unit. For the magnetic endohedral unit we have chosen units of type Mn_4O_4 where Mn is a transition metal. The Mn_4O_4 cluster is usually forms a cubane structure which has been found in single magnetic molecules

such as $Mn_{12}O_{12}$-acetate, Ni_4O_4 single molecule magnets, Co_4O_4-hmp magnetic molecule. Another consideration is that there is charge transfer between the endohedral unit and the carbon cage which stabilizes the whole complex. Typically, in the magnetic molecules there is covalent bonds formed between the cubane core and the outer ligands. The outer organic ligands are typically large and the intermolecular interactions are small. The magnetic molecules form molecular crystals. In the fullerene molecules the carbon cages are large enough to encapsulate the cubane unit. This work is exploratory in nature and our goals are to calculate the spin magnetic moment and the magnetic anisotropy energies of such molecules.

We have chosen two cubane units, Mn_4O_4 and Co_4O_4, as the endohedral unit. The carbon cages we have chosen are C_{70}, C_{76}, C_{78}, and C_{80}. Out of the four cages studied here, only the C_{80} is not stable as a pure carbon cage. The C_{70} cage has an oval shaped structure with D5h symmetry that follows the IPR rule. However, the isomer of the cage in $Sc_3N@C_{70}$ is a non-IPR cage. We have chosen the isomer 7960 which is the non-IPR cage in $Sc_3N@C_{70}$, for encapsulating the Mn4O4 unit. The C_{76} carbon fullerene has D2 symmetry in its isolated structure which follows the IPR rule. However, endohedral DySc2N@C76 has the Cs symmetry. The charge transfer from the endohedral unit plays a significant role on the cage structure. The extra charges on the cages mostly reside on the pentalene units which are formed by fusion of two pentagons. The C_{78} fullerene cage has three stable isomers – one with D3 symmetry and two with C2v symmetry. The encapsulation of the $Sc_3N@C_{78}$ is seen however in a D3h cage, which is an IPR structure. The C_{80} cage has 7 isomers that follows the IPR rule. The endohedral $Sc_3N@C_{80}$ is the most abundant endohedral cluster and can exist

in Ih and D5h symmetry for cage. While selecting the cage structures for encapsulation, we used the cages of the fullerenes in the endohedral form. Therefore, we chose the isomers 7960 for C_{70}, 17490 for C_{76}, 22010 for C_{78}, and isomer 31924 for C_{80} for encapsulation. Here is the table for total number of isomers for each carbon cage.

Table: Cages and number of isomers for each cage

System	Number of isomers	Number of IPR
C70	8149	1
C76	19151	2
C78	24109	5
C80	31924	7

In choosing 31924 isomer for C_{80}, we first choose 300 lowest energy isomer and generate 900 different isomer by rotating endohedral unit. We optimized all of them at PM6 level. We took 10 lowest energy isomer for calculation in DFT level, we found that the lowest energy isomer was 31924.

We have also generated 7 number of isomers for each of the endohedral fullerenes studied here by rotating the endohedral unit about three mutually perpendicular axes by 120 degrees which led to a total number of 28 isomers for a given complex. The complexes are then optimized at the DFT level and their magnetic anisotropy energy is calculated as mentioned in Chapter 2. The optimized structures of the lowest energy isomers of each cluster in the ferromagnetic state are shown in Fig. 4.1.

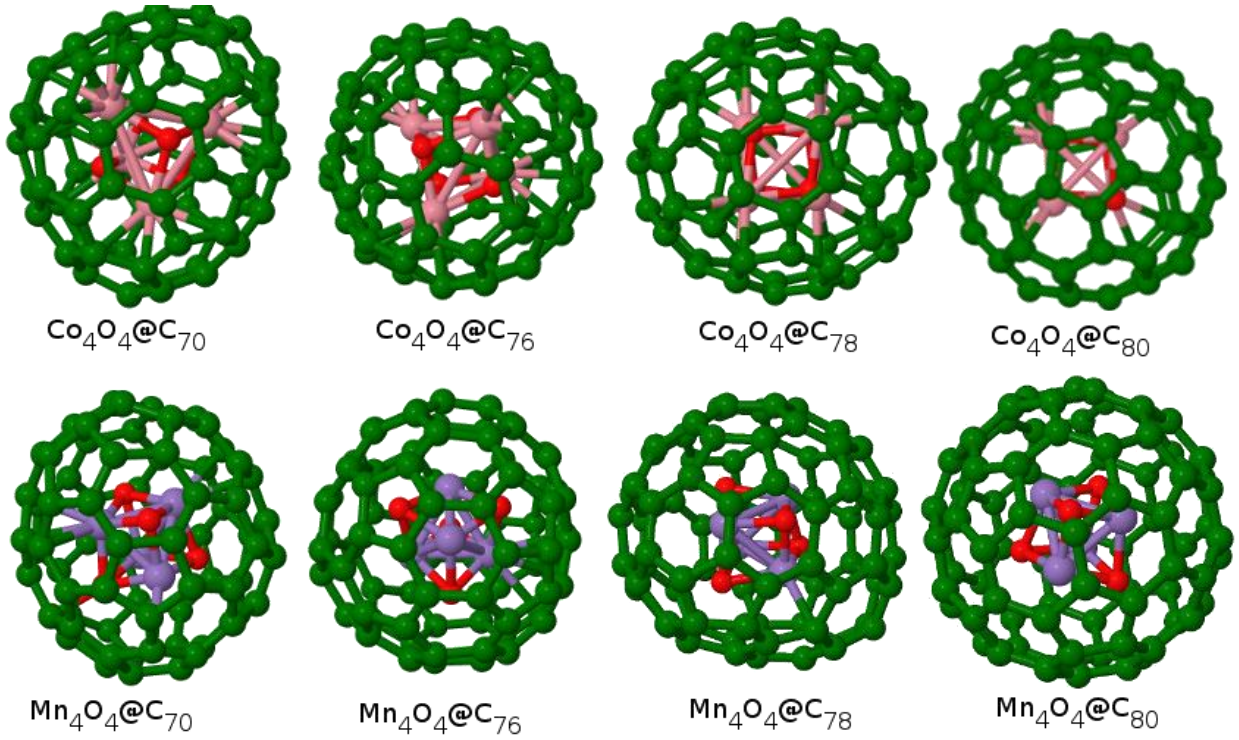

Fig. 4.1. Optimized structures of magnetic endohedral fullerenes.

Co_4O_4 cluster:

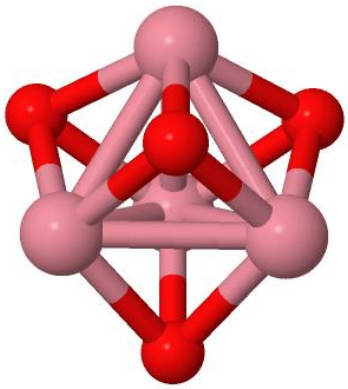

Fig. 4.2 The Co_4O_4 cluster optimized at the PBE-GGA level. The oxygen and Co atoms are shown in red and pink, respectively.

The structure of the isolated Co_4O_4 cluster is tetrahedral with the Co and O atoms forming inverted tetrahedral. The Co atoms in this cluster are in +2 charge state

with a magnetic moment of 3 μ_B per Co atom in a ferromagnetic structure leading to a S=6 spin state for the whole cluster. The O-O average distance is 3.05 A^o and the Co-Co distance is 2.39 A^o which shows that the two tetrahedral are of different sizes. The Co-O distances are 1.95 A^o. The second order magnetic anisotropy energy is however small (0.7K) in this cluster with high symmetry.

$Co_4O_4@C_{70}$

We have optimized 7 isomers in the ferromagnetic state first, generated through rotation of the Co_4O_4 unit along 3 perpendicular directions by 120^o. The difference in the energies of the optimized fullerenes shows that the rotation of the unit is not free inside the C_{70} cage. In the lowest energy ferromagnetic structure we note that the Co atoms are located on top of the hexagons. The Co-C distances, where C atom are from the hexagons near to the Co atom range from 2.13 – 2.93 Ang. The Co atoms form a tetrahedral which is similar to what was earlier found for Co_4O_4 cubane core experimentally (Christou). Bond length in between Co and Co is 2.49 angstrom and O-O is 2.83. The distance between Co and O is 1.8 angstrom.

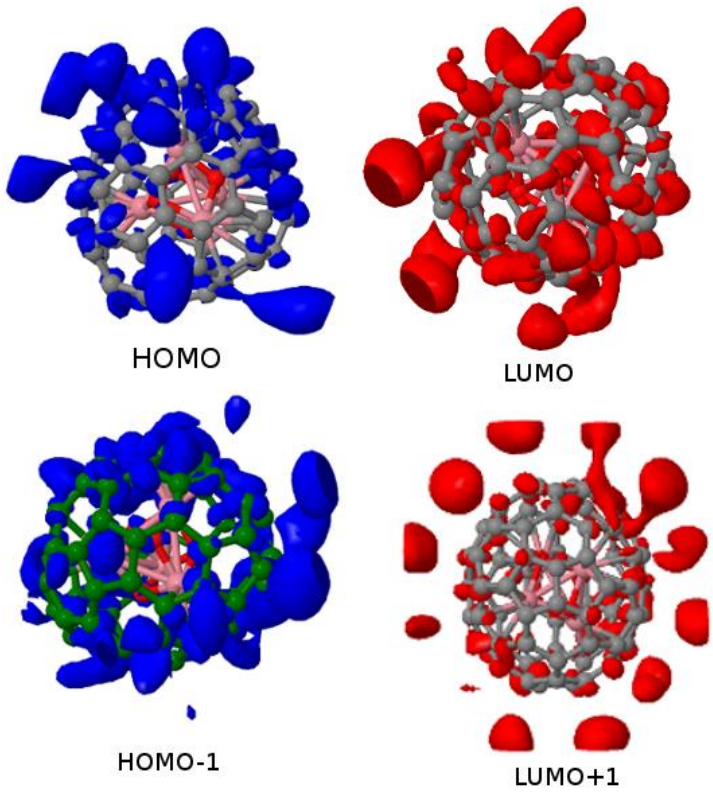

Fig 4.3 HOMO-LUMO plot for the system $Co_4O_4@C_{70}$

The HOMO-LUMO gap of the $Co_4O_4@C_{70}$ system is 0.11 eV which is small. The density of states plot and the plot of the frontier orbitals show the delocalization of these orbitals over both the cage and the endohedral unit. The Co d-orbitals are also shown the DOS plot.

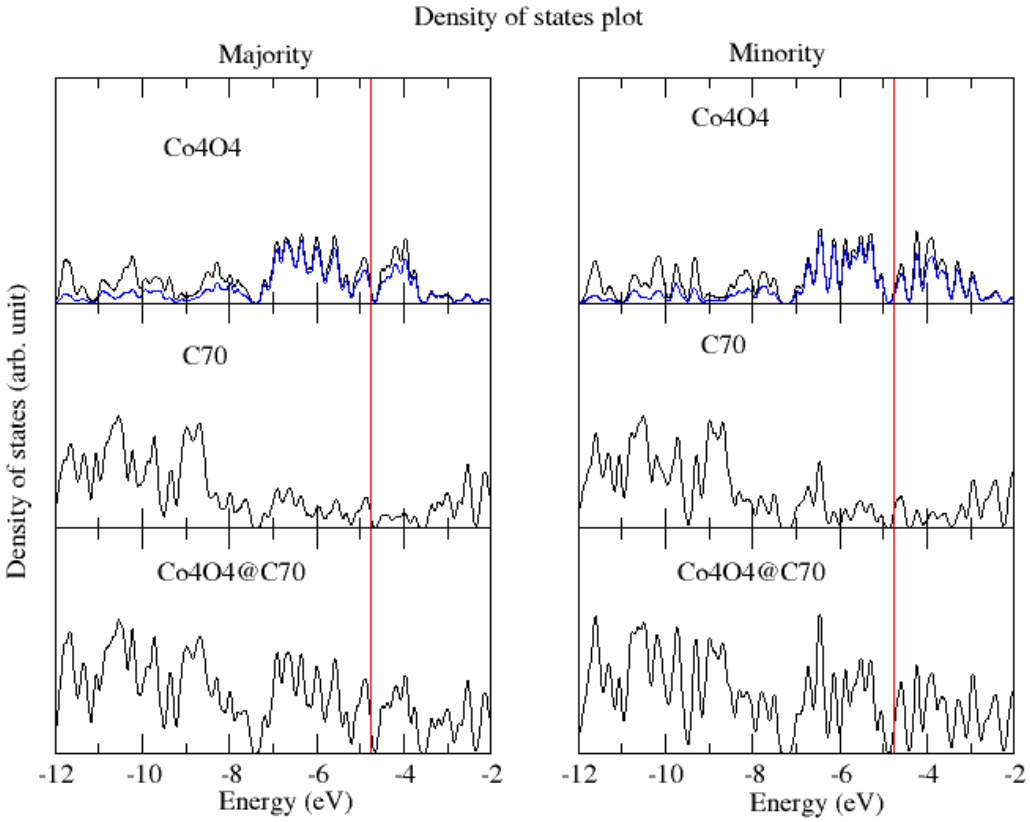

Fig 4.4 Density of States plot for the system $Co_4O_4@C_{70}$

The lowest energy ferromagnetic isomer has a magnetic moment of $4\mu_B$. Considering the nearly identical coordination of all the four Co atoms, it points to a +4 charge state of the Co atoms. Similar conclusions were also reached by Hadt et al. from X-ray absorption spectra of Co_4O_4 cubane (doi.10.1021/jacs.604663). The magnetic anisotropy energy of this complex is small at 9 K and shows a tri-axial magnetic system.

The lowest ferromagnetic state isomer was further studied in an anti-ferromagnetic (AFM) spin ordering. There are 4 Co atoms in the cluster so 7 antiferromagnetic spin ordering is possible which is shown in table below. We find that the anti-ferromagnetic structure, when optimized, reached the same ferromagnetic

solution. One of the Co atom has spin charge 2 around it whereas the other three has small spin charge. The spin charge is spread over the whole Co_4O_4 unit and also over the nearest carbons.

Table 4.1 Data for the system $Co_4O_4@C_{70}$

System(FM)	H-L gap (eV)	M.M. (μ_B)	M.A.E. (K)	Energy (Hartree)
Co4O4@C70	0.11	4	9	-8496.24796

Anti-ferromagnetic calculation:

Calculation	Energy (Hartree)	Spin
AFM1	-8496.240275	↑↓↓↓
AFM2	-8496.240275	↓↑↓↓
AFM3	-8496.240218	↓↓↑↓
AFM4	-8496.240275	↓↓↓↑
AFM5	-8496.240275	↑↑↓↓
AFM6	-8496.240275	↑↓↑↓
AFM7	-8496.240275	↑↓↓↑

$Co_4O_4@C_{76}$

We have chosen the C_{76} cage of isomer 17490 with Cs symmetry for encapsulation. Following the procedure described above we have generated 7 isomers for optimization. We have found two ferromagnetic isomers within an energy separation of 0.007 eV which shows that there are degenerate in energy. However, the complex structures are different and the spin states are also different. In one the structures, the spin magnetic moment is 2 μ_B. In this complex the Co-Co bonds are more stretched up to 3.05 compared to the C_{70} complex and the O-O bonds are 2.4 Angstrom long. In the 7 isomers generated by rotation we note that the magnetic moments have optimized to a range of values from 2 -10 μ_B. Since the lowest energy structures differ only in the spin state, we refer to them as 2 μ_B and 4 μ_B structures. In the 2 μ_B structure, two of the Co atoms cap two hexagonal faces, one caps a pentagonal face and the fourth one is on top of a carbon shared by three hexagons. The density of states of this complex is shown in Fig. 4.5. The DOS near the Fermi level is dominated by the Co d orbitals with some contributions from the carbon p orbitals on the C_{76}. The orbital densities of the frontier orbitals are shown in Fig. 4.6. This complex has a HOMO-LUMO gap of 0.26 eV and the second order magnetic anisotropy energy is 40K.

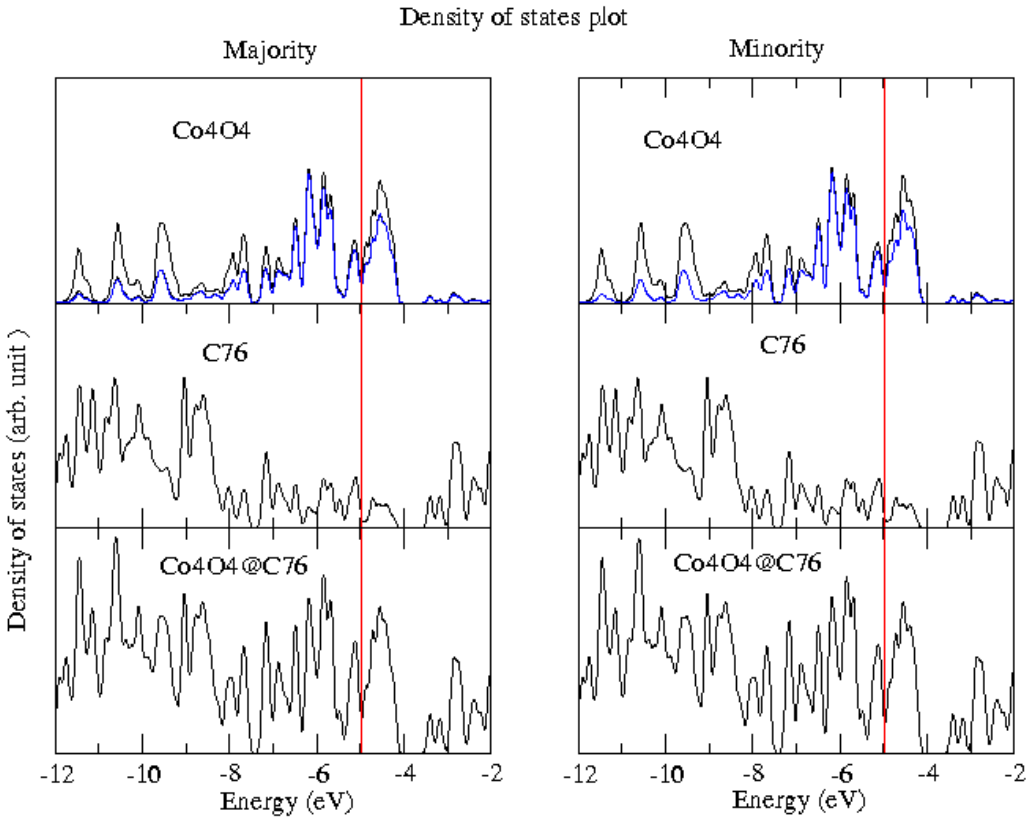

Fig, 4.5. The density of states of the ferromagnetic structure with S=1.

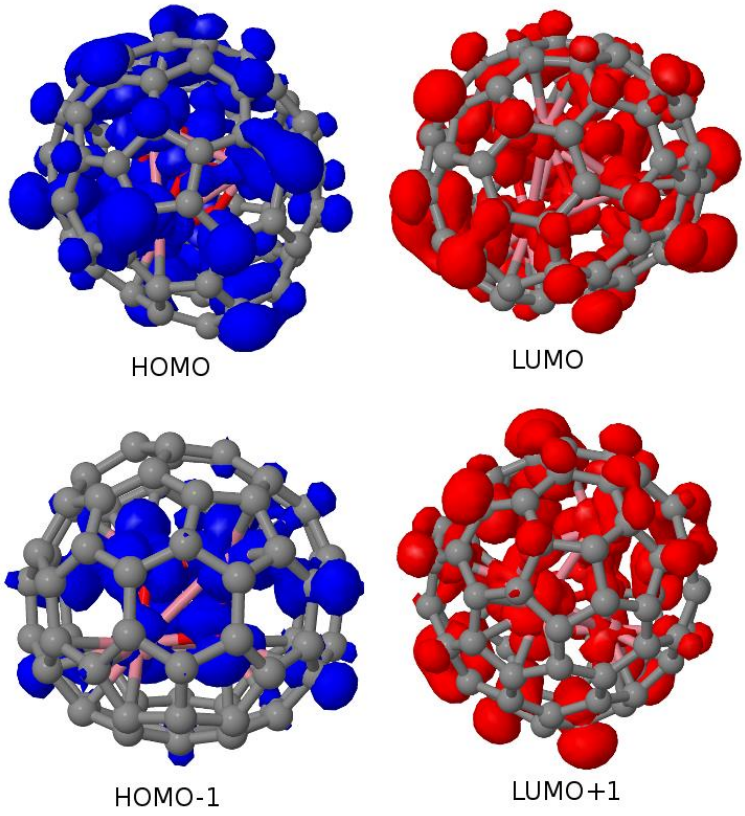

Fig. 4.6. The orbital densities of the HOMO, HOMO-1, LUMO, LUMO+1 of the ferromagnetic lowest energy structure with S=1.

There are 7 AFM spin ordering possible for any of the isomers. We have optimized 7 anti-ferromagnetically ordered states for the lowest energy 2 μ_B complex. We label the complexes as shown in the table and find the lowest energy anti-ferromagnetic structure is the true ground state of the complex. This complex has one Co spin ordered opposite to the other ones. The Co-Co distances range from 2.8 to 3.06 angstron. where the tetrahedral symmetry of the isolated Co_4O_4 is lost. The O-O distances range from 2.34 to 2.47 angstron. The HOMO-LUMO gap in this complex is 0.177 eV and the magnetic anisotropy energy is 17.6 K.

Table 4.2 Data for the System $Co_4O_4@C_{76}$

System(Ferromagnetic)	H-L gap (eV)	M.M. (μ_B)	M.A.E. (K)	Co-Co (A^0)	Energy (Hartree)
Co4O4@C76 (S=1)	0.260	2	40	3.05	-8724.79934

Calculation	Energy (Hartree)	Spin ordering	M. M. (μ_B)
Ferromagnetic S=1	-8724.79934		2
Ferromagnetic S=2	-8724.817079		4
AFM1	-8724.806178	↑↓↓↓	2
AFM2	-8724.808357	↓↑↓↓	4
AFM3	-8724.808301	↓↓↑↓	4
AFM4	-8724.743843	↓↓↓↑	4
AFM5	-8724.792759	↑↑↓↓	4
AFM6	-8724.806050	↑↓↑↓	4
AFM7	-8724.808145	↑↓↓↑	4

System (AFM2)	H-L gap (eV)	M.M. (μ_B)	M.A.E. (K)	Energy (Hartree)
Co4O4@C76	0.177	4	17.01	-8724.808357

$Co_4O_4@C_{78}$

The C_{78} cage has 5 isomers that follow the isolated pentagon rule. Out of these five two isomers have C2v symmetry, another two have D3h symmetry and one has D3

symmetry. The Sc_3N encapsulating C_{78} cage is found to have the isomer number 24109 with D3h symmetry. However, later on it was found that with relatively large Y3N and Lu3N as endohedral unit, the preferred cage structure actually not IPR and has C2 symmetry. The isomer number of this cage is 22010. In the isomer 22010 the endohedral units Y3N and Lu3N are planar. We have used this isomer for encapsulating the Co_4O_4 unit.

We started with 7 ferromagnetic isomers which in the optimized structures have spin magnetic moment ranging from 2 to 8 μ_B. The lowest energy ferromagnetic structure has a mangetic moment of 4 μ_B . Two of the Co atoms cap two hexagonal faces and the other two occupy bridge positions between a hexagon-pentagon bond and a hexagon-hexagon bond. The Co_4O_4 unit is fairly asymmetric with Co-Co bonds ranging from 2.56 to 2.91 A^o. The O-O bonds range from 2.31 to 2.53 A^o.

Table 4.3. Data for the System $Co_4O_4@C_{78}$

System(AFM1)	H-L gap (eV)	M.M. (μ_B)	M.A.E. (K)	Energy (Hartree)
Co4O4@C78	0.178	6	17.275	-8800.951306

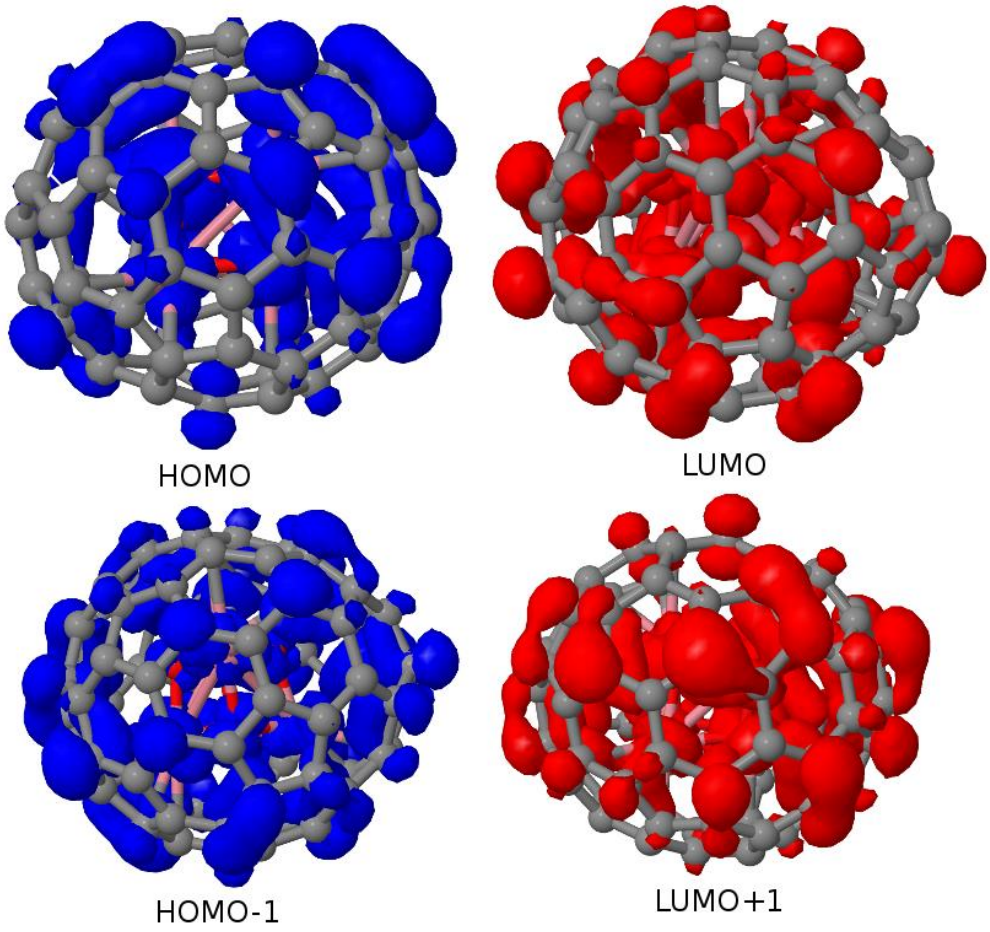
HOMO
LUMO
HOMO-1
LUMO+1

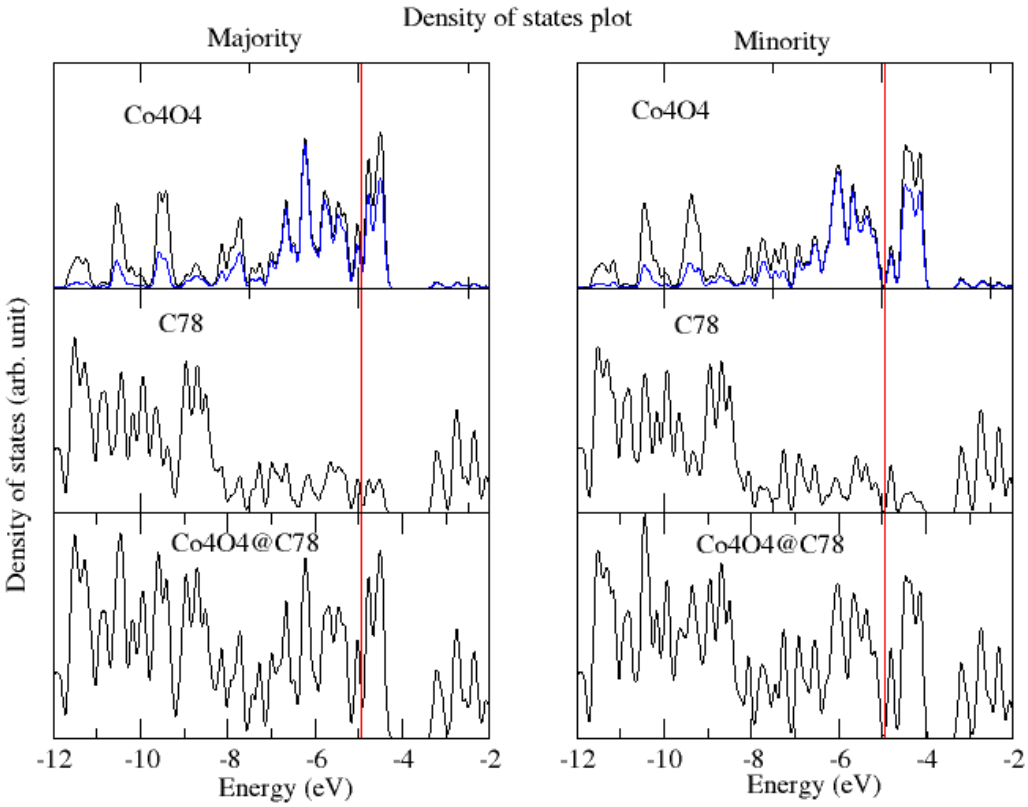

Fig 4.8 Density of States plot for the system $Co_4O_4@C_{78}$

$Co_4O_4@C_{80}$

The C_{80} cage has seven isomers that follow the isolated pentagon rule. These cages have the symmetries Ih, D3, D2, D5h, D5d and two with C2v symmetry. The two most stable endohedral isomers are $Sc_3N@C_{80}$ with Ih and D5h symmetry. Since the experimentally derived endohedral C_{80} fullerenes are found to follow the isolated pentagon rule, we have chosen the Ih structure for encapsulation of the Co_4O_4 cluster. For this complex too we have started with 7 isomers, which were optimized. All the structures optimized to the same spin state with S=3 in the ferromagnetic state. We

have calculated the approximate spin charges on the atoms and find that two of Co atoms have spin moment 3 μ_B located around them whereas the other two Co atoms show comparatively very small but opposite spin charge located around them. The Co4O4 structure is distorted but less than the C_{78} structure. The Co-Co bond lengths vary between 2.79 – 2.94 A^o and the O-O bonds vary from 2.35 – 2.67 A^o. The Co atoms that have small spin charge are closer to the carbon cage with a distance of anout 2.22 A^o from the cage and the other two are further away at 2.37 A^o. The proximity to the cage increases the interaction and reduces the spin charge. This system has a HOMO-LUMO gap of 0.33 eV. The second order magnetic anisotropy energy of the complex is 44.5 K.

Table 4.4. Data for $Co_4O_4@C_{80}$ System

System (AFM1)	H-L gap (eV)	M.M. (μ_B)	M.A.E. (K)	Energy (Hartree)
Co4O4@C80	0.33	4	45.24	-8877.17793

Anti-ferromagnetic calculation:

Calculation	Energy (Hartree)	Spin	M. M. (μ_B)
AFM1	-8877.177935	↑↓↓↓	4
AFM2	-8877.177924	↓↑↓↓	6
AFM3	-8877.166572	↓↓↑↓	2
AFM4	-8877.177084	↓↓↓↑	6

AFM5	-8877.177318	↑↑↓↓	6
AFM6	-8877.177270	↑↓↑↓	6
AFM7	-8877.177084	↑↓↓↑	6

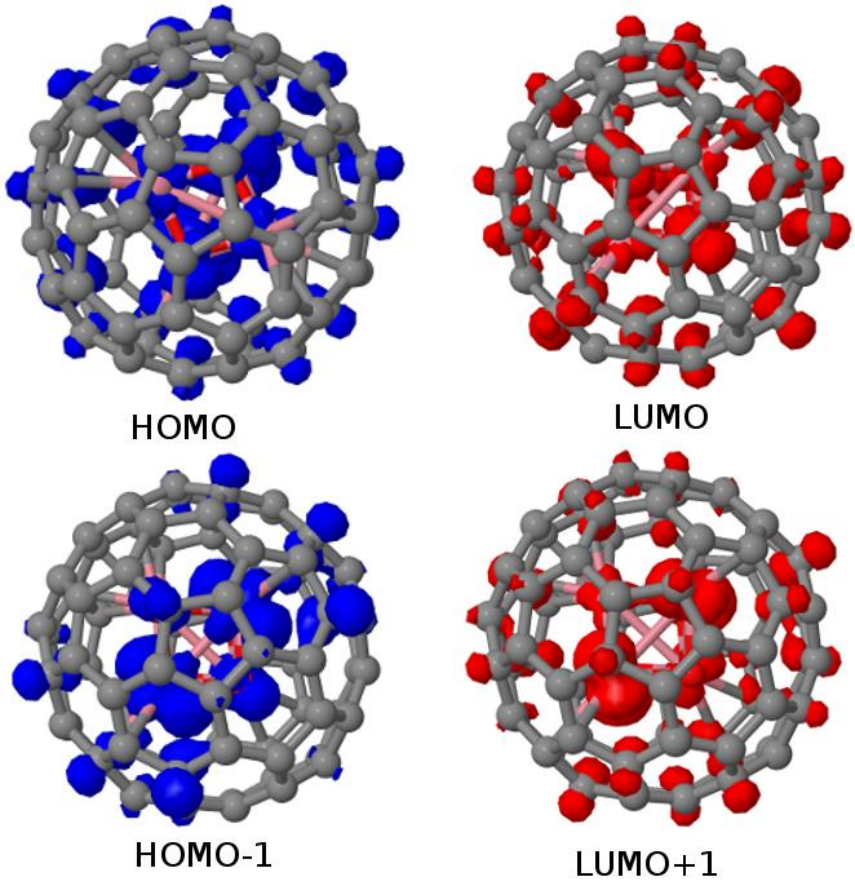

Fig 4.9 HOMO-LUMO plot for the system $Co_4O_4@C_{80}$

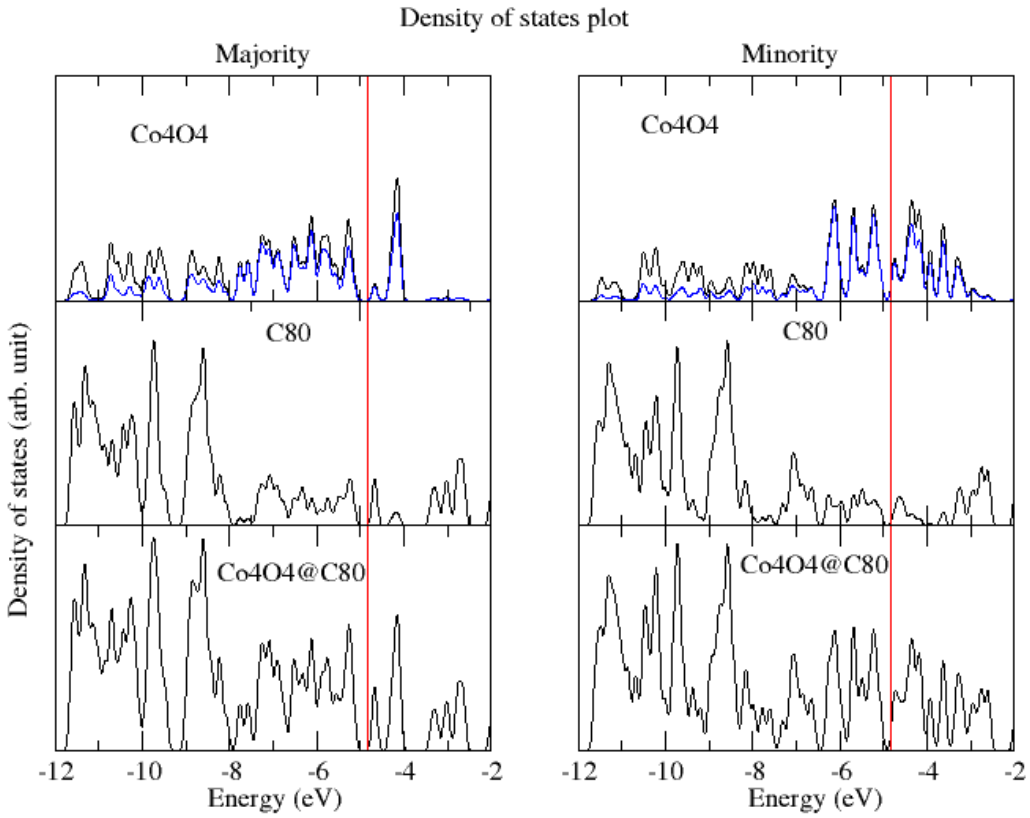

Fig 4.10 Density of states plot for the system $Co_4O_4@C_{80}$

Mn_4O_4:

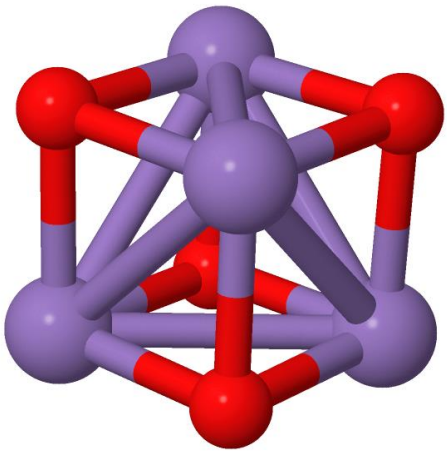

Fig. 4.11: The Mn_4O_4 cubane. The Mn and O atoms are shown as purple and red balls, respectively.

The bare Mn_4O_4 cluster is first optimized at the PBE-GGA level. The ferromagnetic solution shows that the Mn atoms are in +2 charge state and the cluster has a tetrahedral structure each type of atoms forming a tetrahedral. Each Mn is coordinated with three oxygens. The Mn-Mn distances are 2.79 A^0 and the O-O distances are 2.92 A^0 long. The Mn-O bonds are 2.02 A^0 long. The overall spin magnetic moment of the cluster is 20 μ_B. However, the anti-ferromagnetically ordered cluster with zero magnetic moment is more stable by 0.86 eV. In this cluster the Mn are in +3 charge state with 4 μ_B moment per atom. The Mn tetrahedral is slightly distorted with Mn-Mn distances ranging 2.6 – 2.75 A^0 but the O-O distances are more uniform at 2.9 - 3.0 A^0. The Mn-O bonds are 1.95 □^{0} to 2.01 A^0 long. The Mn_4O_4 typically occurs in the (Mn4O4)^+6-L_6 form where the L is a ligand.

$Mn_4O_4@C_{70}$:

We have optimized 7 isomers in the ferromagnetic state first, generated through rotation of the Mn_4O_4 unit by 120^0 along three perpendicular directions. The differences in the energies of the optimized fullerenes shows that the rotation of the encapsulated unit is not free inside the C70 cage. In the lowest energy ferromagnetic structure we note that the two Mn atoms are located on top of the hexagons and other two are connected with pentagons bond ranges from 2.2 to 2.32 angstron. The Mn-C distances, where C atom are from the hexagons near to the Mn atom ranges from 2.29 to 2.42 angstron. Bond length in between Mn and Mn vary from 2.72 to 3.08 angstron and O-O is 2.33 to 2.62 angstron. The distance between Mn and O is 1.79 to 2.13 angstron.

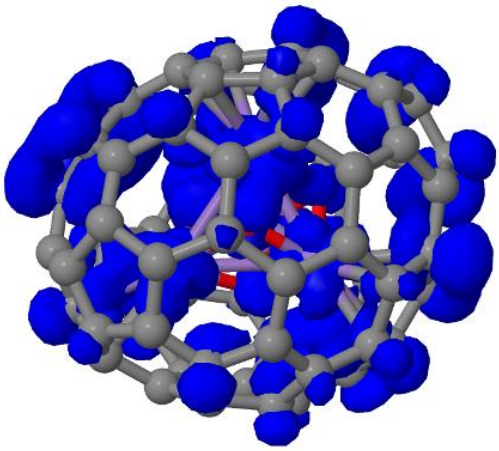

HOMO

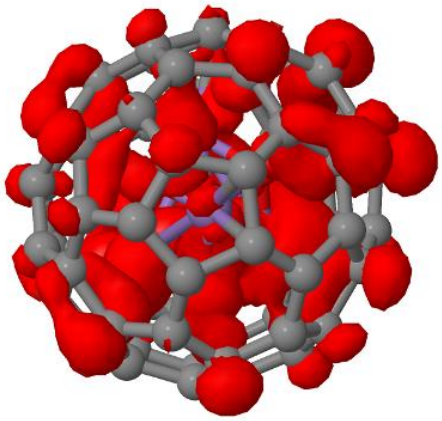

LUMO

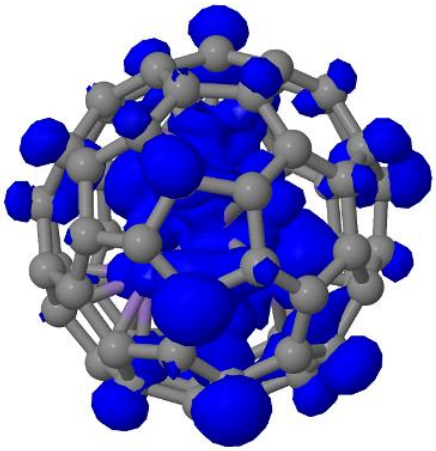

HOMO-1

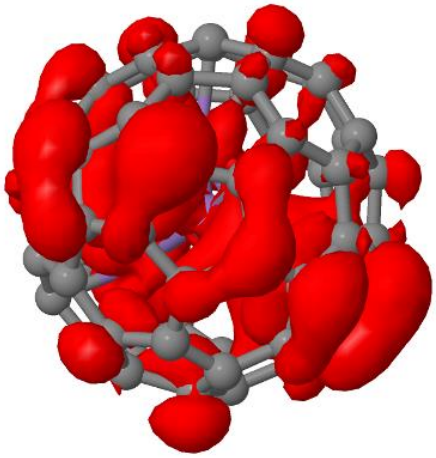

LUMO+1

Fig4.12 HOMO-LUMO plot for the system $Mn_4O_4@C_{70}$

The HOMO-LUMO gap of the $Mn_4O_4@C_{70}$ system is 0.24 eV. The density of states plot and the plot of the frontier orbitals over both the cage and the encapsulated unit. The Mn d-orbitals are also shown in the density of state plot.

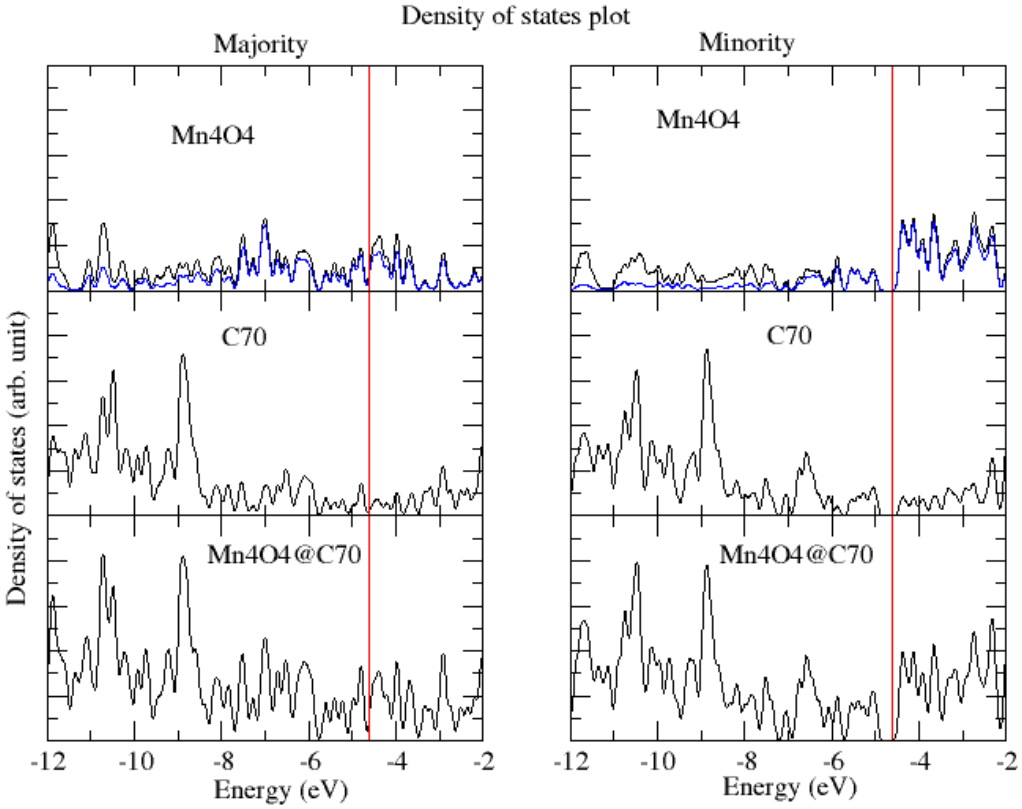

Fig. 4.13 Density of states plot for the system$Mn_4O_4@C_{70}$

The lowest energy ferromagnetic isomer has a magnetic moment 8 μ_B. The magnetic anisotropy energy in this system is 10.54 K. The lowest ferromagnetic state isomer was further optimized in an anti-ferromagnetic (AFM) spin ordering. There are 4 Mn atoms in the clusters so 7 anti-ferromagnetic spin ordering is possible which is shown in table below.

Table 4.5 Data for $Mn_4O_4@C_{70}$ System

System(FMX2)	H-L gap (eV)	M.M. (μ_B)	M.A.E. (K)	Energy (Hartree)
Mn4O4@C70	0.242	8	10.54	-7569.19115

Antiferromagnetic calculation:

Calculation	Energy (Hartree)	Spin	M.M. (μ_B)
1	-7569.186635	↑↓↓↓	8
2	-7569.185920	↓↑↓↓	4
3	-7569.184047	↓↓↑↓	6
4	-7569.179982	↓↓↓↑	4
5	-7569.181152	↑↑↓↓	0
6	-7569.188474	↑↓↑↓	4
7	-7569.184915	↑↓↓↑	2

$Mn_4O_4@C_{76}$

We have chosen the cage C_{76} having isomer number 17490 with Cs symmetry for encapsulation. We have generated 7 isomers for the optimization. In this complex, the spin magnetic moment is 6 μ_B. In this complex the Mn-Mn bonds are 2.77 to 3.02 angstron long. In the 7 isomers generated by rotation we note that the magnetic moments have optimized to a range of values from 4 to 8 μ_B. In this structures, three Mn

atoms cap hexagonal faces and another one with pentagon. The density of states of this system is shown in fig. 14. The density of states near the fermi level is dominated by the Mn d-orbitals with some contribution from the carbon p orbitals from the C_{76} cage. The orbital densities of the frontier orbitals are shown in fig 4.15. This complex has a HOMO-LUMO gap of 0.29 and the second order magnetic anisotropy energy is 17.94 K.

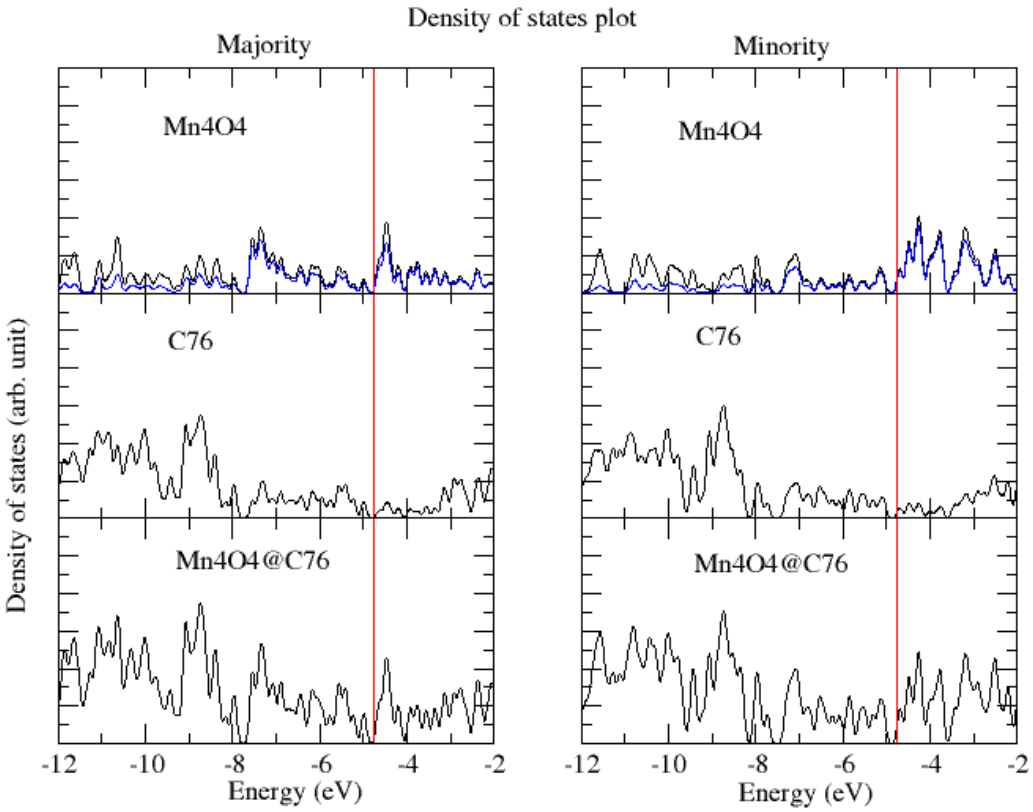

Fig 4.14 Density of States plot for the system $Mn_4O_4@C_{76}$

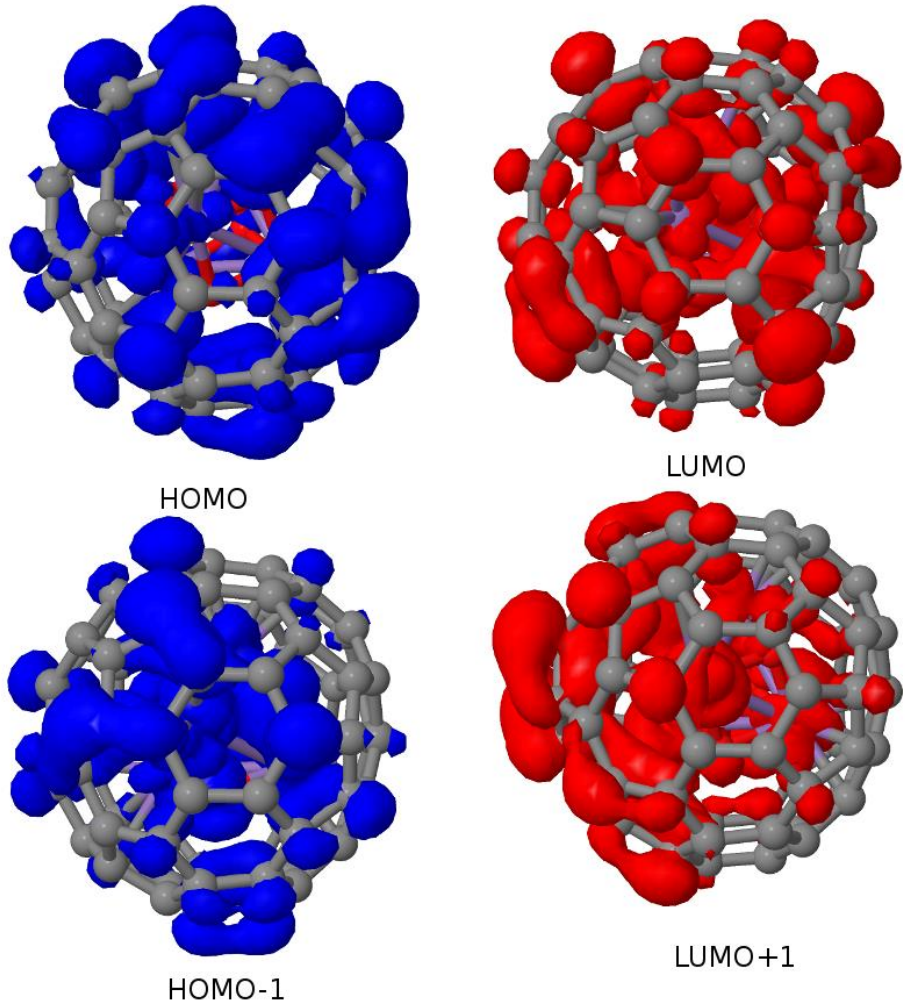

Fig 4.15 HOMO-LUMO plot for the system $Mn_4O_4@C_{76}$

There are 7 AFM spin ordering possible for the lowest energy isomer. We further optimized 7 anti-ferromagnetically ordered states for the lowest energy complex having spin magnetic moments $6\mu_B$. AFM spin ordering data is in table below.

Table 4.6 Data for $Mn_4O_4@C_{76}$ System

System(FMY1)	H-L gap (eV)	M.M. (μ_B)	M.A.E. (K)	Energy (Hartree)
$Mn_4O_4@C_{76}$	0.299	6	17.94	-7797.78004

Antiferromagnetic Calculation for the system Mn4O4@C76:

Calculation	Energy	Spin
AFM1	-7797.76589	↑↓↓↓
AFM2	-7797.76381	↓↑↓↓
AFM3	-7797.75699	↓↓↑↓
AFM4	-7797.76745	↓↓↓↑
AFM5	-7797.76469	↑↑↓↓
AFM6	-7797.76469	↑↓↑↓
AFM7	-7797.76469	↑↓↓↑

$Mn_4O_4@C_{78}$

The C_{78} cage has 5 isomers that follow the isolated pentagon rule. Out of these 5 two isomers have C2v symmetry, another two have D3h symmetry and one has D3 symmetry. The Sc_3N encapsulating C_{78} cage is found to have the isomer number 24109 with D3h symmetry. The isomer number here we used 22010 for encapsulating the Mn_4O_4 unit.

We have 7 isomers generated by rotating the encapsulated unit have spin magnetic moment ranging from 4 to 12 μ_B. The lowest energy ferromagnetic structure has a magnetic moment of 4 μ_B. The Mn_4O_4 unit is fairely assymetric with Mn-Mn bonds ranging from 2.87 to 3.02 angstron. The O-O bonds range from 2.37 to 2.55 angstron.

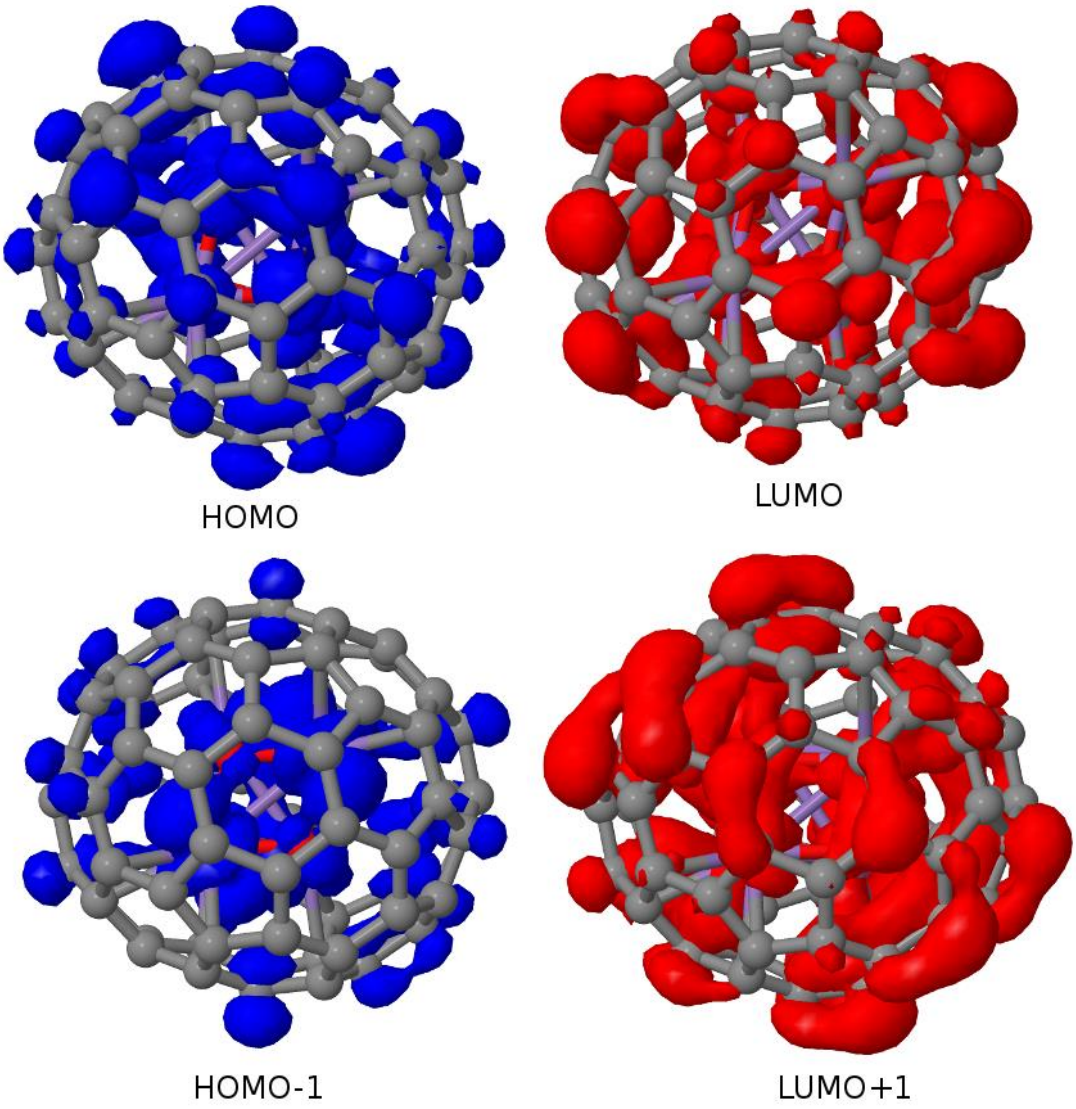

Fig 4.16 HOMO-LUMO plot for the system $Mn_4O_4@C_{78}$

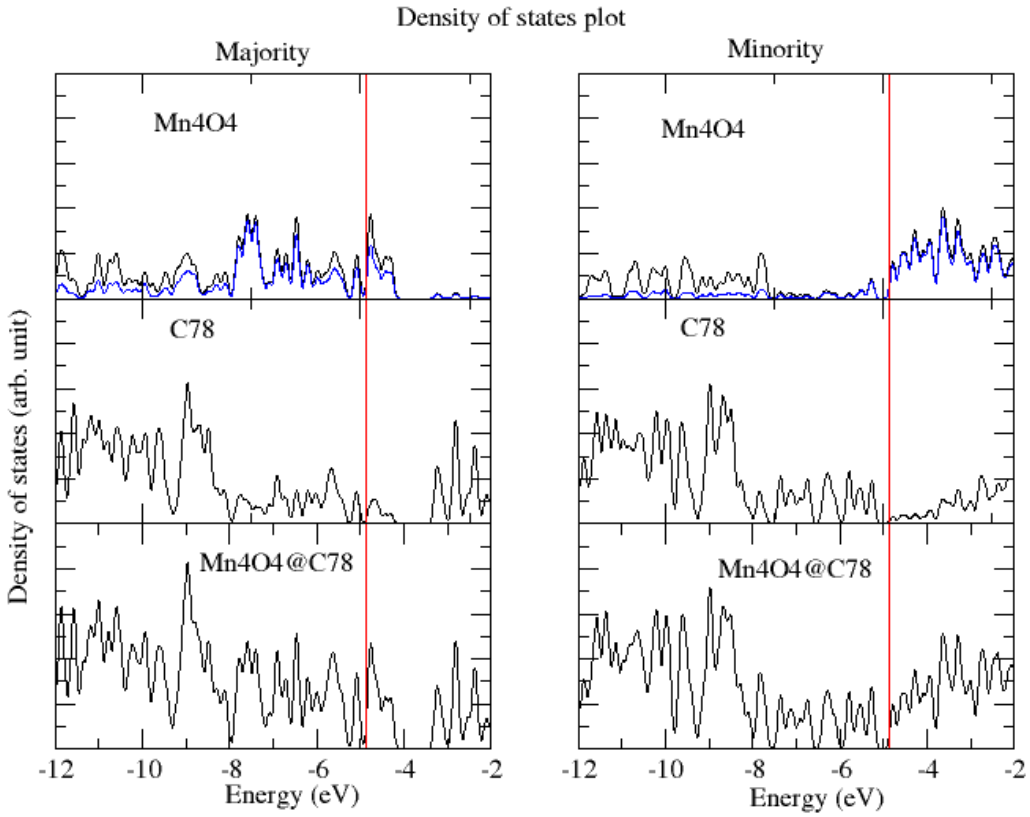

Fig 4.17 Density of States plot for the system $Mn_4O_4@C_{78}$

Table 4.7 Data for $Mn_4O_4@C_{78}$ System

System(FMY2)	H-L gap (eV)	M.M. (μ_B)	M.A.E. (K)	Energy (Hartree)
Mn4O4@C78	0.264	4	42.82	-7873.93632

Antiferromagnetic calculation

Calculation	Energy (Hartree)	Spin	M.M. (μ_B)
AFM1	-7873.93087	↑↓↓↓	6
AFM2	-7873.93087	↓↑↓↓	6
AFM3	-7873.93108	↓↓↑↓	8
AFM4	-7873.93087	↓↓↓↑	8
AFM5	-7873.93087	↑↑↓↓	2
AFM6	-7873.93087	↑↓↑↓	0
AFM7	-7873.93087	↑↓↓↑	0

$Mn_4O_4@C_{80}$

The C_{80} cage has seven isomers that follow the isolated pentagon rule. These cages have the symmetries Ih, D3, D2, D5h, and two with C2v symmetry. The two most stable endohedral isomers are $Sc_3N@C_{80}$ with Ih and D5h symmetry. Since the experimentally resultant endohedral C_{80} fullerenes are found to follow the IPR, we have chosen the Ih structure for encapsulation of the Mn_4O_4 unit. Also for this system we have generated 7 isomers for the ferromagnetic spin state, which were optimized. The Mn-Mn bonds vary between 2.51 to 2.53 angstron and the O-O bonds vary from 2.72 to 2.74 angstron. This system has a HOMO-LUMO gap 0.14 eV, which is small. The second order magnetic anisotropy energy of the complex is 2.96 K.

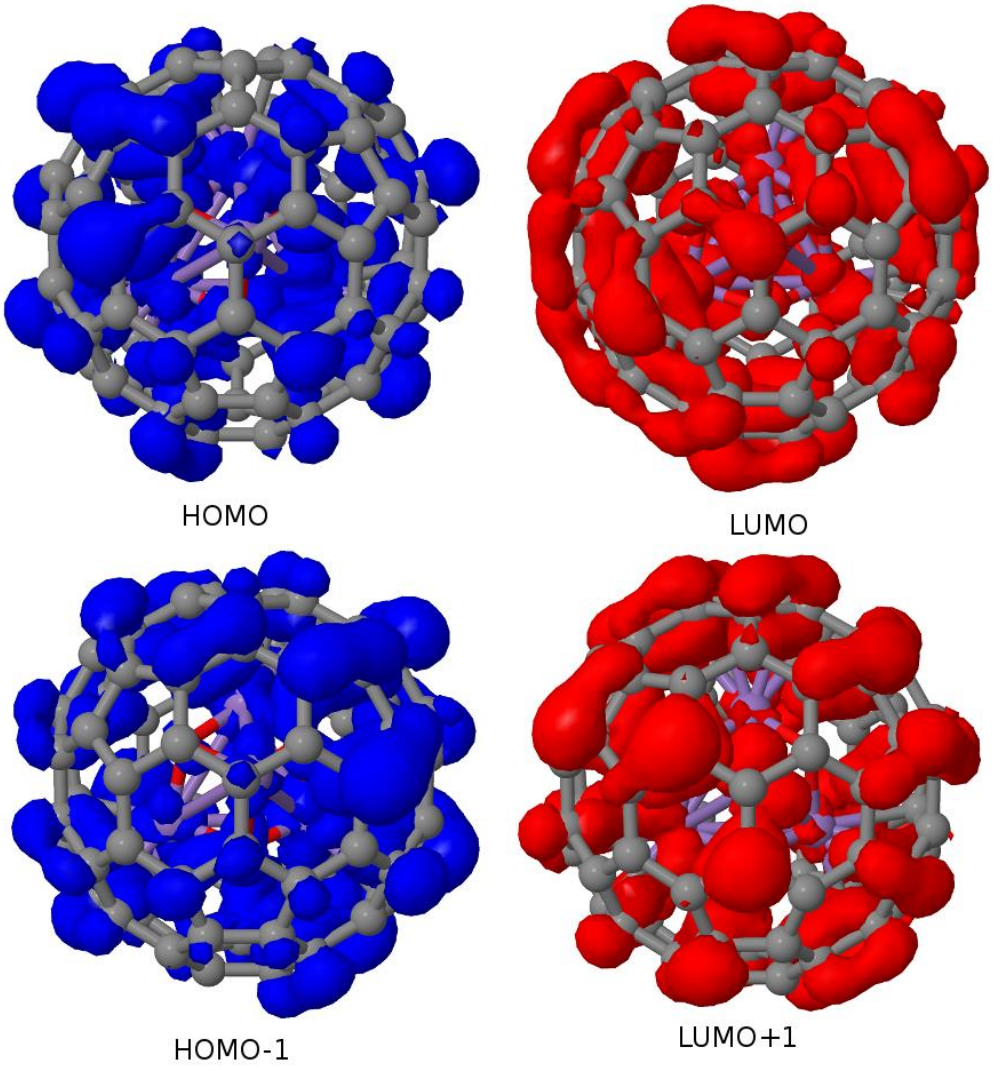

Fig 4.18 HOMO-LUMO plot for the system $Mn_4O_4@C_{80}$

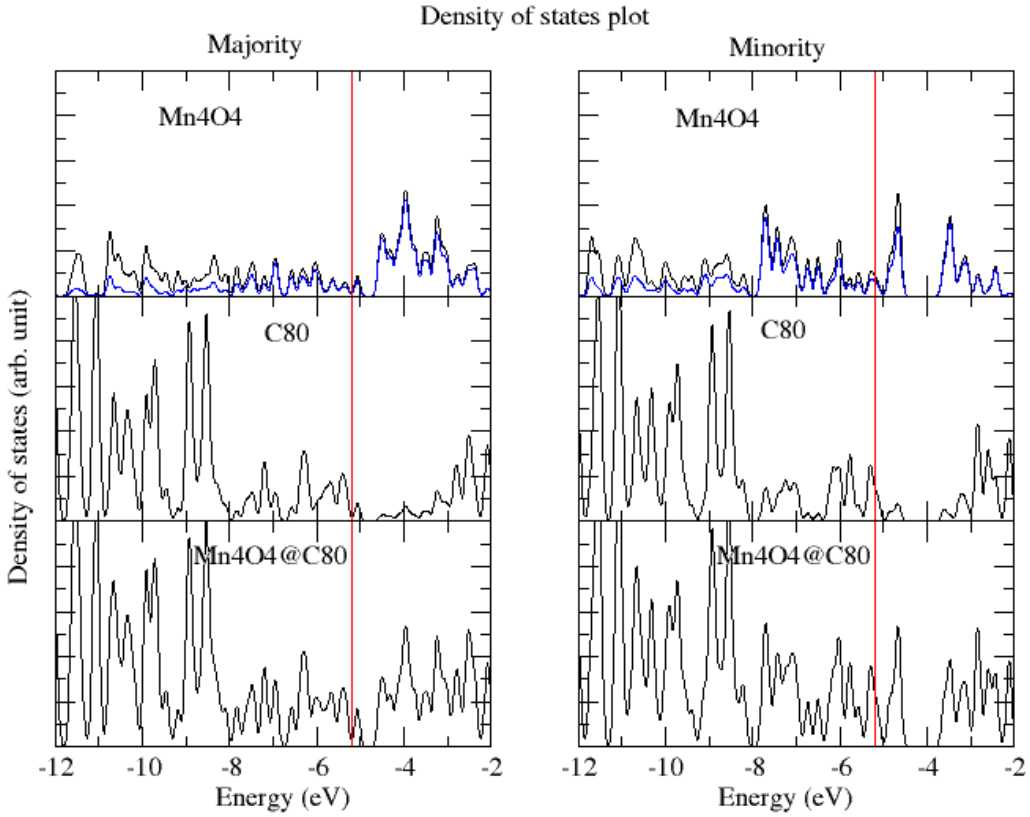

Fig 4.19 Density of States plot for the system Mn4O4@C80

Table 4.8 Data for $Mn_4O_4@C_{80}$ System

System(FMX3)	H-L gap (eV)	M.M. (μ_B)	M.A.E. (K)	Energy (Hartree)
Mn4O4@C80	0.146	2	2.96	-7950.0568

Antiferromagnetic calculation:

Calculation	Energy	Spin
AFM1	-7950.19064	↑↓↓↓

AFM2	-7950.19061	↓↑↓↓
AFM3	-7950.19067	↓↓↑↓
AFM4	-7950.19061	↓↓↓↑
AFM5	-7950.19064	↑↑↓↓
AFM6	-7950.19065	↑↓↑↓
AFM7	-1950.19061	↑↓↓↑

CHAPTER 5

CONCLUSION

Using the accurate density functional calculation we predict that the system with Co_4O_4 and Mn_4O_4 clusters can exist as stable magnetic endohedral fullerenes. The magnetic anisotropy energy in $Co_4O_4@C_{70}$, $Co_4O_4@C_{76}$, $Co_4O_4@C_{78}$ and $Co_4O_4@C_{80}$ is 9, 40, 17.25 and 44.5 K respectively. And for the Mn4O4 cluster we found that the most favorable isomer is in FM state and anisotropy energy is 10.54,17.94, 42.82 and 2.96 K respectively, but in Co4O4 first two $Co_4O_4@C_{70}$ and $Co_4O_4@C_{76}$ are in ferromagnetic state and other two $Co_4O_4@C_{78}$ and $Co_4O_4@C_{80}$ are in anti-ferromagnetic state. In parent clusters the magnetic anisotropy energy was low because of high symmetry so in EMFs we found that the increase in MAE.

CHAPTER 6

SIC APPLICATION

The self-interaction correction method outlined in Chapter 3 based on the Fermi Lowdin orbitals is a variational method in which the total energy of the system can be minimized through variation of the Fermi orbitals and through variation of the Kohn-Sham orbitals. In practice, this leads to optimization of the Fermi orbital descriptor positions. Our goal here is to apply the FLO-SIC scheme to FeO_4 cluster for which the DFT functionals predict a spin state different from the MR method. However, to understand how the FOD positions change we have first applied it to a few closed shell atoms at the Hartree, LDA-exchange only and LDA exchange-correlation levels. We have applied it to Be, Ne, Mg and Ar atoms.

Be atom

The Be atom has the shell structure $1s^2 2s^2$ and therefore requires only two positions of FODs for each spin. The Fermi orbitals in this case are close to the Kohn-Sham orbitals in that one is related to the 1s orbital and the second one is related to the 2s orbital. We have noted the general trend that the position of the FOD for the 1s orbital is same as that of the nucleus which makes is easy to determine the position of the 1s orbital. The position of the second FOD that pertains the 2s orbital can be placed isotropically around the atom. We have first carried out the total energy calculations within the Hartree approximation only. Since the position of the 2s FOD can be isotropic we have incrementally changed the position and calculated the total energy. The total energy vs. the FOD position curve is shown in Fig. 4.20. In the Hartree approximation, the total energy is minimum with the second FOD at 1.905 Bohr from the

center. To obtain the exchange-only position we started from the 1.905 Bohr position of the second FOD. The exchange–only calculations with SIC led to a point 3.602 Bohr away from the center. Simillarly after including the LDA correlation as given in the PW91 approximation, the optimized FOD position was found at 3.605 Bohr. This picture is consistent with the exchange interaction since it removes electrons of parallel spin from around an electron. The correction to coulomb energy is 2.656 Hartree in the absence of any exchange interaction. The exchange-only energy is 2.316 Hartree and the exchange-correlation energy is 2.547 Hartree.

Table 4.9 Data for the atom Beryllium

Atom	Hartree	Exchange only +SIC	LDA Exchange-Correlation+SIC	Expt.
Be	-14.563 (2.656)	-14.589 (0.371)	-14.706 (0.264)	-14.667

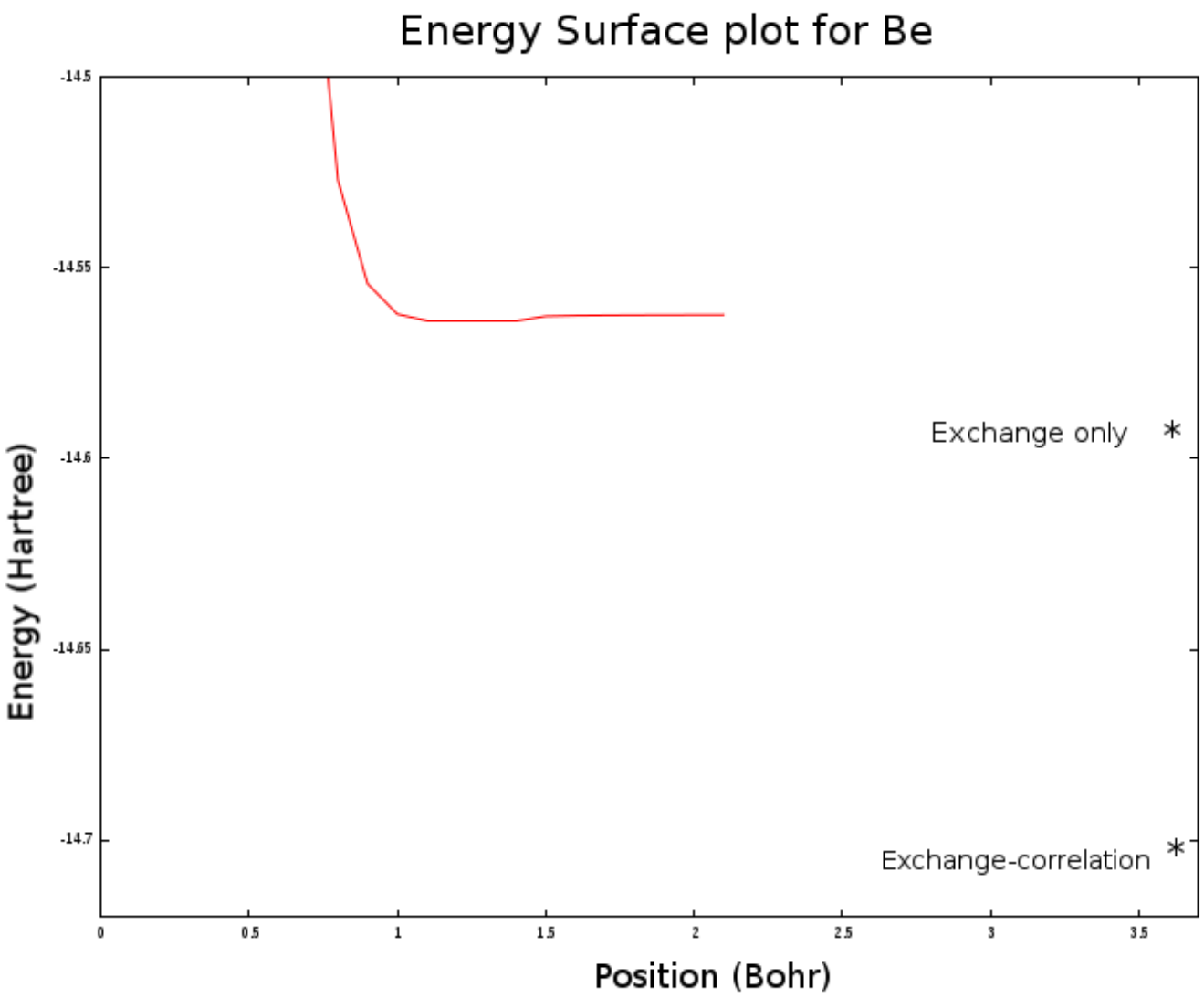

Fig. 4.20 Energy vs 2nd FOD position plot for the atom Be

Neon atom

The Ne atom has the shell structure $1s^2 2s^2 2p^6$ and therefore requires only five positions of FODs for each spin. The Fermi orbitals in this case are one is related to the 1s-centroid was placed at the origin and the second one 2sp were placed at the vertices of the tetrahedron. We have noted the general trend that the position of the FOD for the 1s is same as that of the nucleus which makes is easy to determine the position of the 1s orbital. The position of the second FOD, that is 2sp orbital can be placed at the vertices

of tetrahedron by symmetry operation. We have first carried out the total energy calculations within the Hartree approximation only. Since the position of the second FOD (2sp) that is vertices of the tetrahedron can be symmetric so we have incrementally changed the distance from origin to vertices of the tetrahedron and calculated the total energy. The total energy vs. the FOD position curve is shown in the Fig.4.21. In the Hartree approximation, the total energy is minimum with the 2sp FOD at 0.66 Bohr from the center. To obtain the exchange-only position we started from the 0.66 Bohr position of the 2sp FOD. The exchange–only calculations with SIC led to a point 1.08 Bohr away from the center. Simillarly, after including the LDA correlation as given in the PW91 approximation, the optimized FOD position was found at 1.10 Bohr. This picture is consistent with the exchange interaction since it removes electrons of parallel spin from around an electron.

Atom	Hartree	Exchange only+SIC	LDA Exchange-Correlation+SIC	Expt.
Ne	-127.371 (9.934)	-128.864 (1.36)	-129.280 (1.03)	-128.938

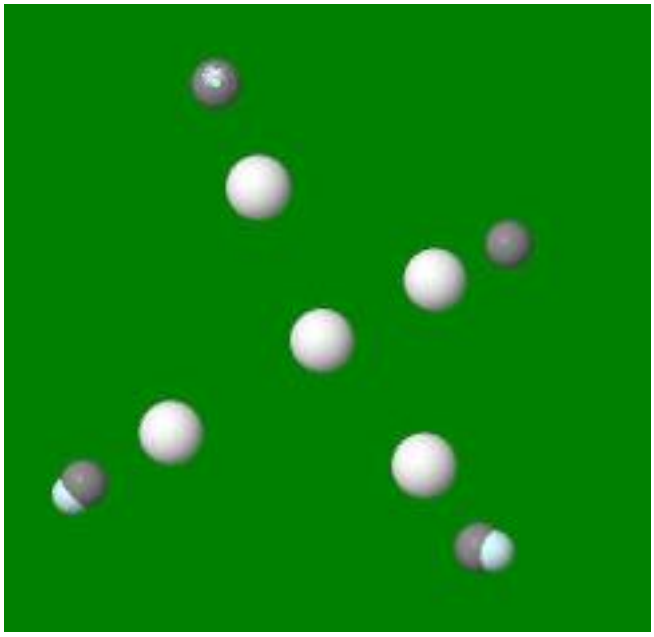

Fig. FOD plot for Ne

Argon atom

The Ar atom has the shell structure $1s^2 2s^2\ 2p^6\ 3s^2\ 3p^6$ and therefore requires only nine positions of FODs for each spin. The Fermi orbitals in this case are one is related to the 1s-centroid was placed at the origin, the second one 2sp-centroid were placed at the vertices of the 1st tetrahedron and the third one 3sp fermi orbital also the vertices of 2nd tetrahedron structure. We have noted the general trend that the position of the FOD for the 1s is same as that of the nucleus which makes is easy to determine the position of the 1s orbital. The position of the second FOD, that is 2sp orbital can be placed at the vertices of tetrahedron by symmetry operation and the third one is also the vertices of 2^{nd} tetrahedron. We have first carried out the total energy calculations within the Hartree approximation only. Since the position of the second (2sp) and the third (3sp) FOD that is vertices of the tetrahedron can be symmetric so we have incrementally changed the distance from origin to vertices of the 1^{st} and 2^{nd} tetrahedron position and calculated the

total energy. The total energy vs. the FOD position that surface plot curve is shown in the Fig. 4.21. In the Hartree approximation, the total energy is minimum with the 2sp FOD at 0.311 Bohr away from the center and 3sp FOD at 1.24 Bohr from the center. To obtain the exchange-only position we started from the 0.311 Bohr position of the 2sp FOD and 1.24 Bohr position of the 3sp FOD. The exchange–only calculations with SIC led to a point 0.380 Bohr away from the center to the first tetrahedron and 1.34 Bohr away from the centre to the second tetrahedron. Similarly after including the LDA correlation as given in the PW91 approximation, the optimized FOD position was found at 0.39 Bohr for 2sp FOD and 1.34 Bohr for 3sp FOD. The correction to coulomb energy is 25.863 Hartree in the absence of any exchange interaction. The exchange-only energy is 2.582 Hartree and the exchange-correlation energy is 3.20 Hartree.

Atom	Hartree	Exchange only +SIC	LDA Exchange-Correlation+SIC	Expt.
Ar	-522.670 (25.863)	-527.741 (2.582)	-528.536 (3.20)	-527.544

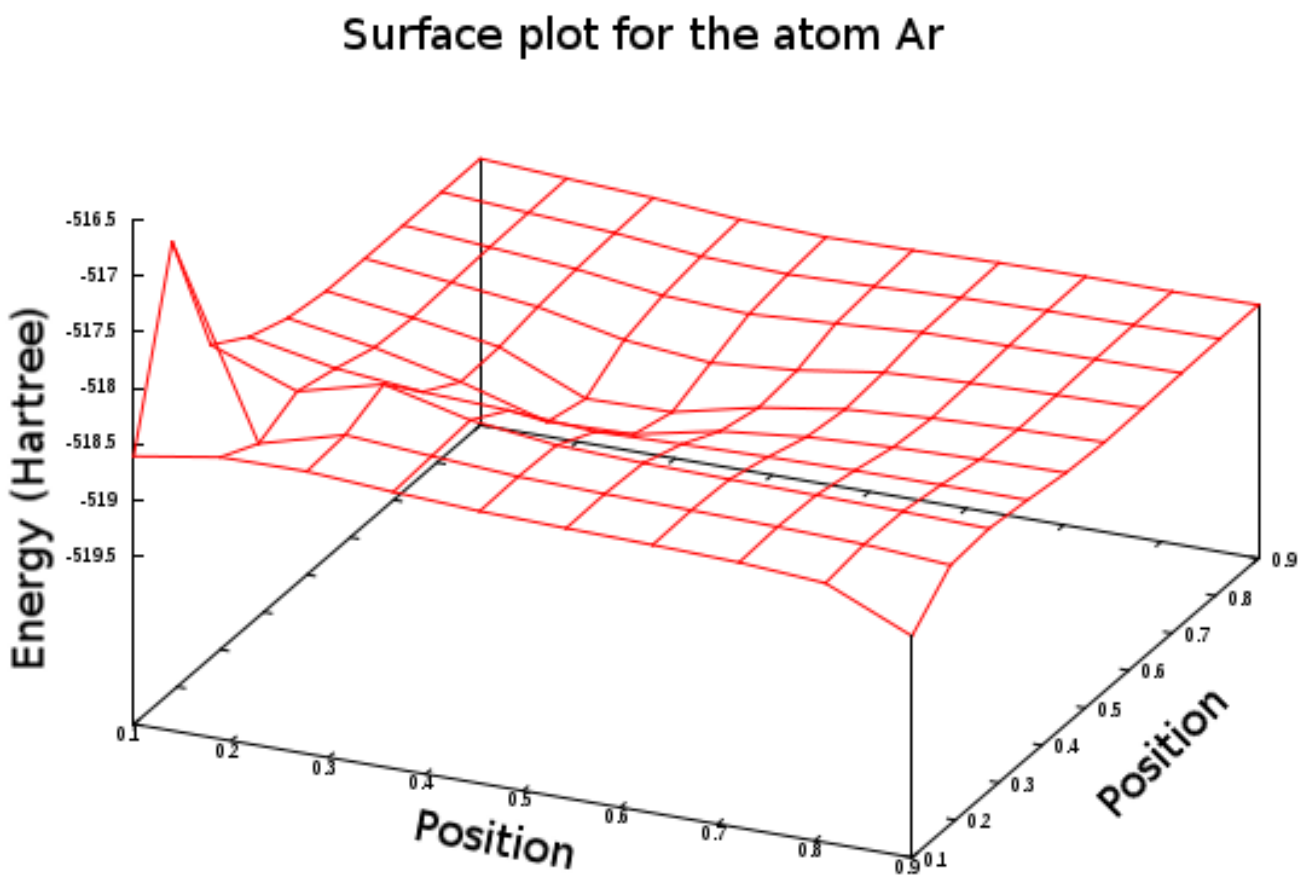

Fig. 4.22 Surface plot for the atom Ar

Magnesium Atom

Atom	Hartree	Exchange only	LDA Exchange-Correlation	Expt.
Mg	196.400 (12.558)	199.423 (1.372)	199.933 (0.987)	200.054

The Mg atom has the shell structure $1s^2 2s^2\ 2p^6\ 3s^2$ and therefore requires only six positions of FODs for each spin. It is found that the position viewed as a tetrahedron with an additional FO capping one of the triangular faces. The surface plot for this atom is as shown in fig.4.23.

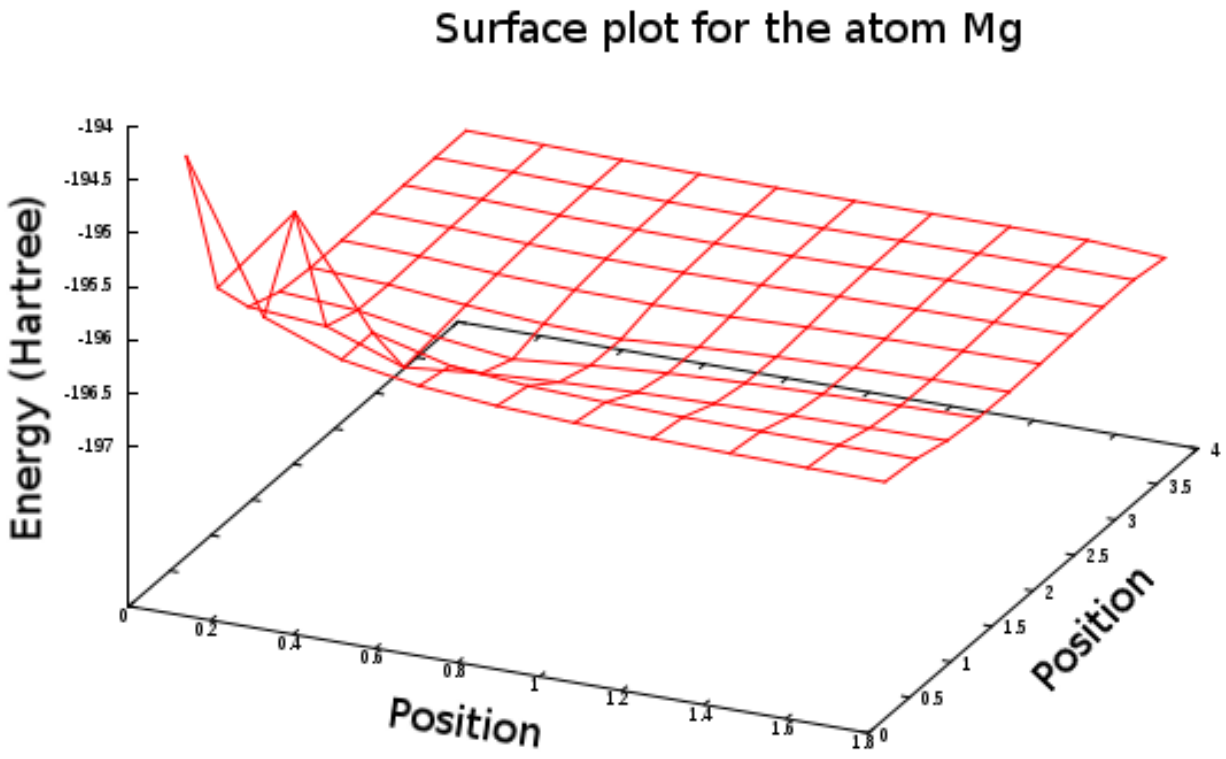

Future Work

1. Our goal here is to apply the FLO-SIC scheme to FeO_4 cluster for which the DFT functional predict a spin state different from the MR method, so we will apply this method to the molecules:

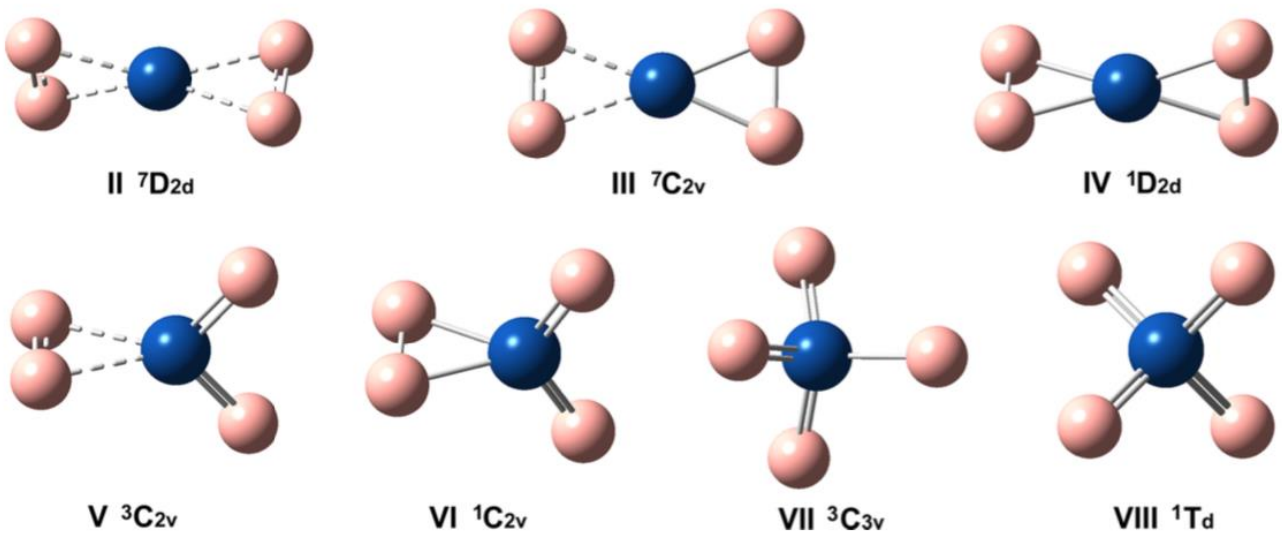

Fig. Stationary Fe-4O isomers: molecular structure, oxidation state of Fe (II-VIII), and spin multiplicity (7-1).

REFERENCES

1. Jones, R O Introduction to Density Functional Theory and Exchange-Correlation Energy Functionals, NIC Series, Vol. 31, 2006
2. Tu, Guangde Studies of Self-interaction Corrections in Density Functional Theory, 2008
3. Kroto H W, Heath J R, O'Brien S C, Curl R F and Smalley R E, Buckminsterfullerene, Nature 318: 162-3, 1985
4. Yan Chai, Ting Guo, Changming Jin, Robert E. Haufler, L. P. Felipe Chibante, Jan Fure, Lihong Wang, J. Michael Alford and Richard E. Smalley, Fullerene with Metals Inside, 1991
5. Diamagnetism and Paramagnetism. Retrived from http://users.aber.ac.uk/ruw/teach/334/diapara.php
6. Hartree- Fock Theory Retrived from http://vergil.chemistry.gatech.edu/notes/quantrev/node28.html
7. David Sherril C. An Introduction to Hartree-Fock Molecular Orbital Theory, June 2000
8. Juan Carlos Cuevas, Introduction to Density Functional Theory. Retrived from https://www.uam.es/personal_pdi/ciencias/jcuevas/Talks/JC-Cuevas-DFT.pdf
9. Jack Simons, Electronic structure theory-Density functional theory. Retrived from https://www.youtube.com/watch?v=3Kv-m4XeX-c.[Video-file]
10. Variational method wiki: https://en.wikipedia.org/wiki/Variational_method_(quantum_mechanics)

11. Variational Theory and the variational principe retrived from http://www.nyu.edu/classes/tuckerman/quant.mech/lectures/lecture_3/node1.htm
12. Variational Method retrived from http://vergil.chemistry.gatech.edu/notes/quantrev/node28.html
13. Nabil M. R. Hoque, Tunna Baruah, J. Ulises Reveles and Rajendra Zope, Challenges and Advances in Computational Chemistry and Physics, Vol. 23 Magnetic Anisotropy Energy of Transition Metal Alloy Clusters
14. Magnetic Anisotropy Energy Retrived from https://en.wikipedia.org/wiki/Anisotropy_energy
15. Jens Kortus, Mark R. Pederson, Tunna Baruah, N. Bernstein, C.S. Hellberg, Density functional studies of single molecules magnets
16. Perdew J. P. and Zunger A., Self-interaction Correction to Density Functional Approximations for many electron systems, Phys. Rev. B 23, 5048,1981
17. Mark R. Pederson, Fermi Orbitals Derivatives in self-interaction corrected density functional theory: Application to closed shell atoms
18. Zeng-hui Yang, Mark R. Pederson and John P. Perdew Full Self-Consistency in the Fermi-Orbital Self-interaction Correction, 2017
19. Mark R. Pederson and Tunna Baruah, Self-interaction corrections within the fermi orbital based formalism.

VITA

Kamal Nyaupane was born in Nepal. He completed his Bachelor of science and Masters of science in physics from Tribhuvan University which is the top ranked University in Nepal. He joined at the University of Texas at El Psao in January 2015 as a graduate student. He got the opportunity to work as a Research Assistant and Teaching Assistant in computational science program at the University of Texas at El Paso.

Permanent address: Shaligram, 9 Setibeni Parbat
Nepal

This thesis/dissertation was typed by Kamal Nyaupane.